activated by the cardiomyocyte-specific α-myosin heavy chain (αMHC) promoter (Figure 1A, Figure S1). EGFRdn mice exhibited heart failure and died at 5–30 weeks of age (Figure 1B). Gross inspection of the EGFRdn hearts showed global chamber dilatation with marked wall thinning (Figure 1C). The heart/body weight ratio was approximately 1.5-fold higher at 6 weeks of age in EGFRdn mice than in wild-type mice (Figure 1D). Echocardiography showed a significant decrease in the fractional shortening (FS) together with chamber dilatation (Figure 1E). In the second model, cardiomyopathy was induced by intraperitoneal injection of doxorubicin in wild-type mice. Doxorubicin-induced cardiomyopathy (DOX) mice showed marked dilatations of the left ventricular diastolic and systolic dimensions, and reduction of cardiac function (Figure S2).

Intravenous infusion of BMMNC transiently improved the cardiac function in DCM mice

BMMNC (2.0×10^7 cells) were isolated from wild-type healthy mice and intravenously infused *via* the tail veins to 8-week-old EGFRdn mice and 11-week-old DOX mice. An equal volume of PBS was infused into control mice. Three days after infusion, echocardiography showed that the FS was significantly improved in BMMNC-treated EGFRdn (Figure 2A) and DOX (Figure 2A) mice, compared with the respective controls. However, these effects were lost by 14 d after infusion (Figure 2A). When the infusion was repeated every 2 weeks, cardiac function showed improvements for >50 d (Figure 2B).

Although infusion of BMMNC is not promising for the treatment of heart failure, we may be able to apply alternative treatment if we understand the underlying mechanisms of beneficial effects of BMNNC infusion. To elucidate the mechanisms, we infused BMMNC derived from GFP mice. Although many GFP-positive cells were observed in the peripheral blood and the spleen at 3 d after infusion (Figure 2C, D), none were found in the heart, lung, liver, kidney or skeletal muscle (Figure 2E). At day 14, few GFP-positive cells were observed even in the peripheral blood (Figure 2C). This was consistent with the observation that BMMNC infusion improved cardiac function at day 3, but not at day 14. These results suggest that BMMNC infusion improves the systolic function of DCM mice not by transdifferentiation of BMMNC into cardiomyocytes but probably by humoral factors secreted from BMMNC. Size of each cardiomyocyte was larger in BMMNC-infused EGFRdn mice than in PBS-infused EGFRdn mice when infusions were repeated every 2 weeks for 8 weeks (i.e.,

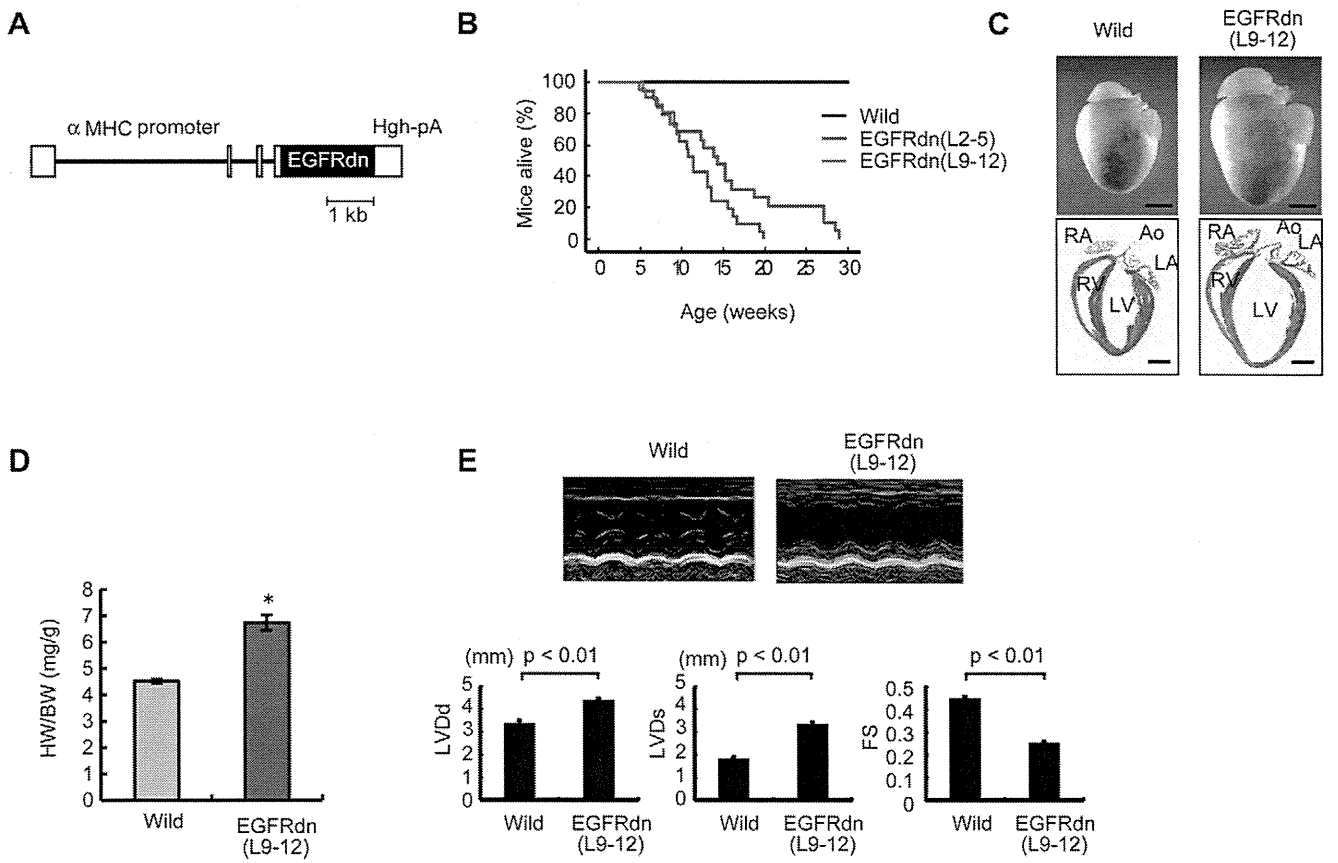

Figure 1. Transgenic overexpression of EGFRdn in the heart causes progressive heart failure. (A) Schematic representation of the cDNA construct used to generate EGFRdn mice. The construct contains an αMHC promoter, human EGFRdn cDNA and a human *growth hormone* polyadenylation signal (Hgh-pA). (B) Kaplan-Meier survival curves for wild-type ($n=62$) and EGFRdn (L2–5, $n=19$; L9–12, $n=21$) mice, showing a significant reduction in the survival rates in EGFRdn mice (log rank test, $P<0.0001$). (C) Gross morphology of whole hearts (upper panels) and longitudinal sections (lower panels) of hearts from wild-type and EGFRdn mice (L9–12) at 6 weeks of age. Ao, aorta; LA, left atrium; LV, left ventricle; RA, right atrium; RV, right ventricle. Scale bars: 2 mm. (D) Heart-to-body weight ratios (HW/BW) of wild-type ($n=9$) and EGFRdn (L9–12, $n=7$) mice at 6 weeks of age. *$P<0.01$. (E) Echocardiographic analysis. The upper photographs show representative M-mode images. The lower graphs show the left ventricular diastolic and systolic dimensions and FS of 8 week-old EGFRdn mice (L9–12) ($n=23$) and age-matched wild-type mice ($n=10$). LVDd, left ventricular diastolic dimension; LVDs, left ventricular systolic dimension. Data are means ± s.e.m.
doi:10.1371/journal.pone.0027901.g001

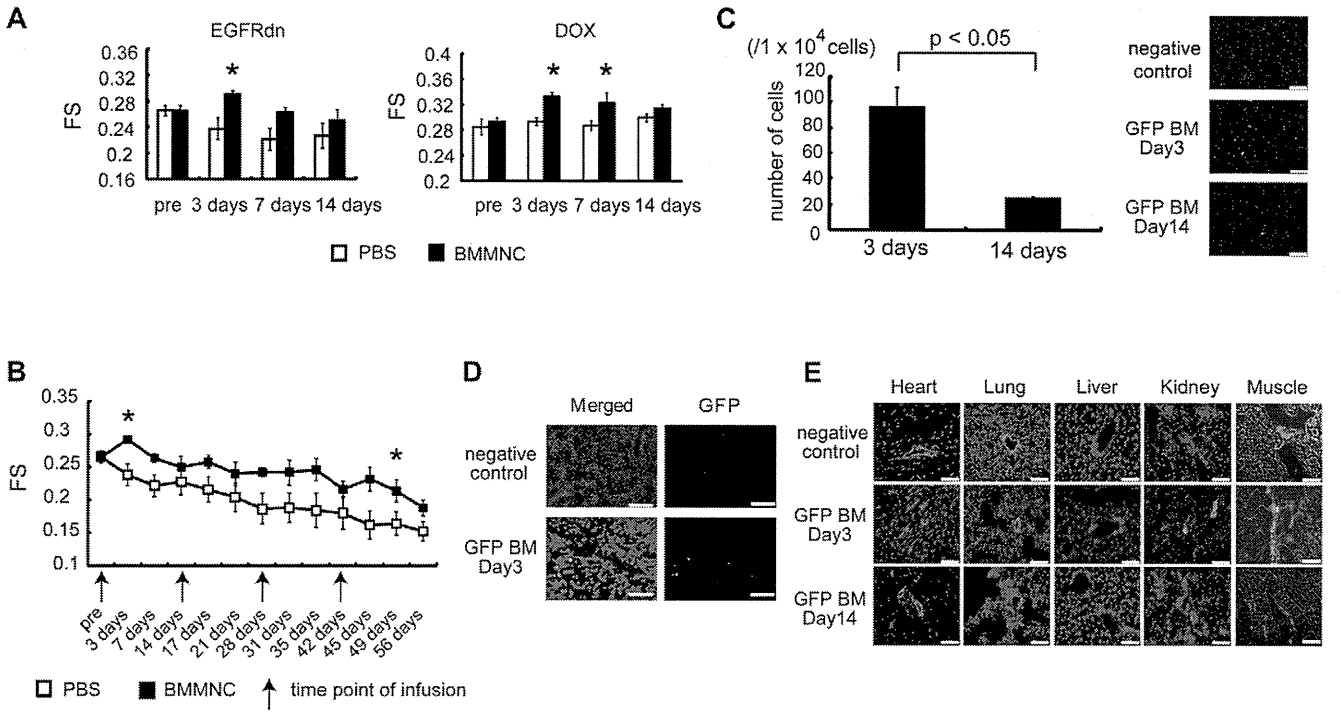

Figure 2. BMMNC infusion transiently improved the cardiac function of DCM mice. (A) Echocardiographic analysis. Transient improvements of FS were observed at 3 d in the BMMNC-treated group, but not the control (PBS) group, in EGFRdn mice (left), and at 3 and 7 d in DOX-treated mice (right). *$p<0.05$ versus PBS ($n=8$ per group). (B) Repeated-infusion experiments. BMMNC were infused every 2 weeks. A similar pattern of improvement in FS was observed after each infusion. *$p<0.05$ versus PBS ($n=8$ per group). (C–E) Immunohistochemical analysis. (C) Left, the number of GFP-positive BMMNC in peripheral blood ($n=3$). Right, photomicrographs of peripheral blood. Nuclei were stained with Hoechst 33258 (blue). Scale bars, 75 μm. (D) Images of the spleen 3 d after infusion. Many GFP-positive cells were observed in the spleen (lower photographs). Upper photographs, negative control. Nuclei were stained with Hoechst (blue color). Scale bars, 25 μm. (E) No GFP-positive cells were observed in any organs. Upper photographs, negative control. Middle and lower photographs, images taken at 3 and 14 d, respectively, after infusion. The vessels were stained with smooth muscle cell actin (red). Nuclei were stained with Hoechst 33258 (blue). The photographs of muscle are merged fluorescent and phase-contrast images. Scale bars, 75 μm. Data are means ± s.e.m.
doi:10.1371/journal.pone.0027901.g002

4 injections) (Figure S3). There were no changes in capillary density or the number of apoptotic cells in the heart between the BMMNC-infused group and the control group (data not shown).

BMMNC-derived conditioned medium (CM) improved cardiomyocyte contractility

To elucidate whether factors secreted from BMMNC were involved in their beneficial effects on cardiac function, we first examined the effects of CM from BMMNC on the contractility of cultured cardiomyocytes of neonatal rats. After serum starvation for 12 h, cardiomyocytes were challenged with culture medium conditioned by BMMNC. Cell shortening was significantly enhanced and beating rate was markedly increased at 30 min and at 12 h after starting culture with the CM, compared with those in untreated cells (Figure 3A), suggesting that BMMNC secrete factors that positively affect cardiomyocyte contractility. Flow cytometric analysis revealed that BMMNC consisted of several cell populations including myeloid (Gr-1(+) cells, ~40%), erythroid (TER119(+) cells, ~20%), and lymphoid cells (B220(+) cells, ~20%) (Figure S4). The individual cell populations, including the lineage-negative population of cells, were sorted by magnetic beads. The isolated cells were 0.8×10^7 Gr-1(+) cells, 0.4×10^7 B220(+) cells, 0.2×10^7 TER(+) cells, and 0.1×10^7 lineage-negative cells from 2.0×10^7 BMMNC. When CM was collected from each population and added to cardiomyocytes starved for 12 h, only the CM from Gr-1(+) cells significantly enhanced cell shortening and increased the beating rate (Figure 3B), suggesting that Gr-1(+) cells mainly contribute to BMMNC-mediated improvements in cardiomyocyte contractility. CM from Gr-1(+) cells or BMMNC isolated from wild-type mice also induced significant hypertrophy of cardiomyocytes (Figure S5). We next examined the effects of CM from Gr-1(+) cells on DOX mice. At 1 and 3 d after the infusion of CM from Gr-1(+) cells, FS was significantly improved, as with infusion of BMMNC (Figure 3C). Furthermore, +dp/dt, as determined by catheterization of the left ventricle, was also improved at 1 d after the infusion, as compared with the control group (Figure 3D). Collectively, these results indicate that factors secreted from Gr-1(+) cells are responsible for BMMNC-induced improvements in cardiac function in DCM mice.

Analysis of factors secreted from Gr-1(+) cells

The CM from wild-type Gr-1(+) cells significantly enhanced cell shortening and increased the beating rate, while CM from EGFRdn Gr-1(+) cells had marginal effects (Figure 4A). This suggests that the factors that improve cardiomyocyte contractility are more abundant in cells of wild-type mice than cells of EGFRdn mice. We next performed DNA microarray analysis to identify the factors involved in these effects. Twenty three genes showed enhanced expression in Gr-1(+) cells from wild-type mice compared with EGFRdn mice (Table 1). The gene which showed the largest difference between two types of mice was growth

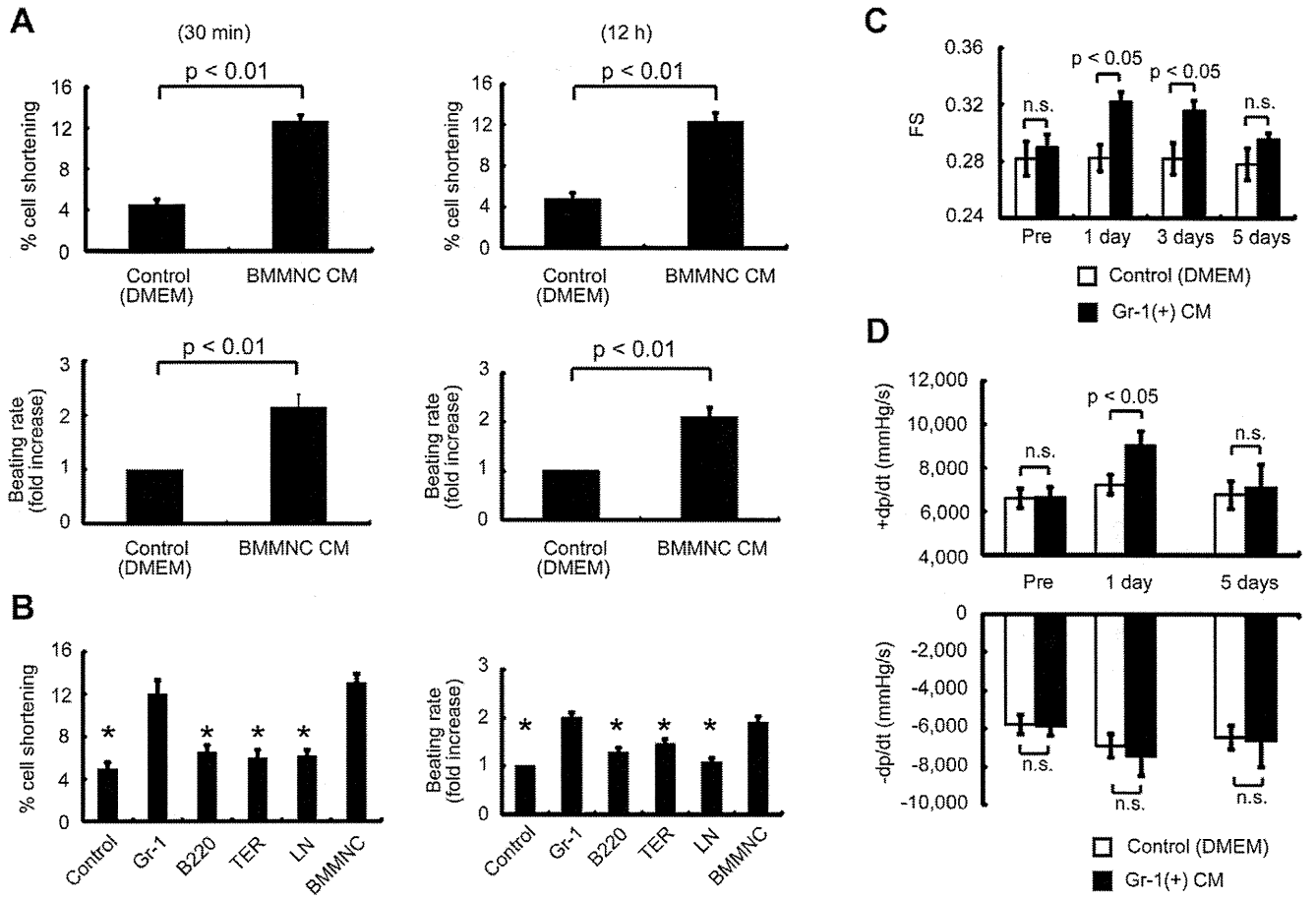

Figure 3. BMMNC-derived CM directly affects cardiomyocyte contractility. (A) Cell shortening and the beating rate of neonatal rat cardiomyocytes were significantly increased after exposure to CM from BMMNC compared with the control ($n = 26$ cells per group). The left and right graphs show the results at 30 min and at 12 h after treatment, respectively. Upper graph, cell shortening. Lower graph, beating rate. (B) CM from Gr-1(+) cells improved the cell shortening and increased the beating rate similar to that achieved by CM from BMMNC ($n = 27$ per group). (C, D) Effects of CM from Gr-1 cells on cardiac function *in vivo*. (C) Echocardiographic analysis ($n = 7$). The infusion of CM from Gr-1(+) cells significantly improved the FS of DOX mice at 1 and 3 d. (D) Infusion of CM from Gr-1(+) cells significantly improved the +dp/dt of DOX mice at 1 d, *in vivo* ($n = 7$). n.s., not significant. Data are means ± s.e.m.
doi:10.1371/journal.pone.0027901.g003

hormone (GH). The reduced expression of GH in Gr-1(+) cells from EGFRdn mice was confirmed by quantitative RT-PCR and ELISA (Figure 4B, C). GH levels were also lower in CM from Gr-1(+) cells isolated from old myocardial infarction (OMI) mice and DOX mice (Figure S6) than in CM from wild-type mice. Consistent with the downregulation of GH secretion from Gr-1(+) cells of heart failure mice, the serum GH levels were also lower in models of heart failure such as DOX, EGFRdn and OMI mice than in wild-type mice (Figure 4E).

Critical role of GH in Gr-1(+) cell-mediated cardioprotection

We examined the role of GH in the effects of Gr-1(+) cell-derived CM using pegvisomant, a specific inhibitor of the GH receptor [12]. Treatment with pegvisomant abolished the enhanced cell shortening and the increased beating rate induced by CM from Gr-1(+) cells (Figure 5A), while the anti-IGF-1 antibody had no effects (Figure 5B). These results suggest that Gr-1(+) cells improved the cardiomyocyte contractility *via* GH, but not *via* IGF-1 *in vitro*. CM from Gr-1(+) cells activated various signaling molecules, including Akt, extracellular signal-regulated kinase (Erk) 1/2, Janus kinase (Jak) 2, signal transducers and activators of transcription (Stat) 3/5 and protein kinase A (PKA) in cardiomyocytes (Figure 5C), and these effects were completely abolished by pegvisomant (Figure 5C). The addition of GH (500 pg/ml), a concentration equivalent to that in the CM from wild-type Gr-1(+) cells, activated the same signaling molecules (Figure 5C), suggesting that CM from Gr-1(+) cells activates Akt, Erk1/2, Jak2, Stat3/5 and PKA through the GH receptor signaling. Furthermore, the CM from Gr-1(+) cells, as well as GH, increased the amount of cyclic AMP (cAMP) in cardiomyocytes, which was also inhibited by pegvisomant (Figure 5D). The improvements in cardiac function induced by CM from Gr-1(+) cells were also abolished by treatment with the GH inhibitor (Figure 5E), whereas the anti-IGF-1 antibody had no effects (Figure 5F). Furthermore, the infusion of CM from Gr-1(+) cells increased the GH levels in serum of DCM mice (Figure 5G). These results suggest that Gr-1(+) cells improve the cardiac contractility *in vivo* also through GH. The BMMNC-mediated improvement in cardiac function of OMI mice was also affected by treatment with pegvisomant (Figure S7), suggesting that GH in BMMNC might have the therapeutic effects on heart failure caused by various etiologies.

Since Stat 3 is one of the important downstream targets of the GH receptor in cardiomyocytes (Figure 5C), we examined the

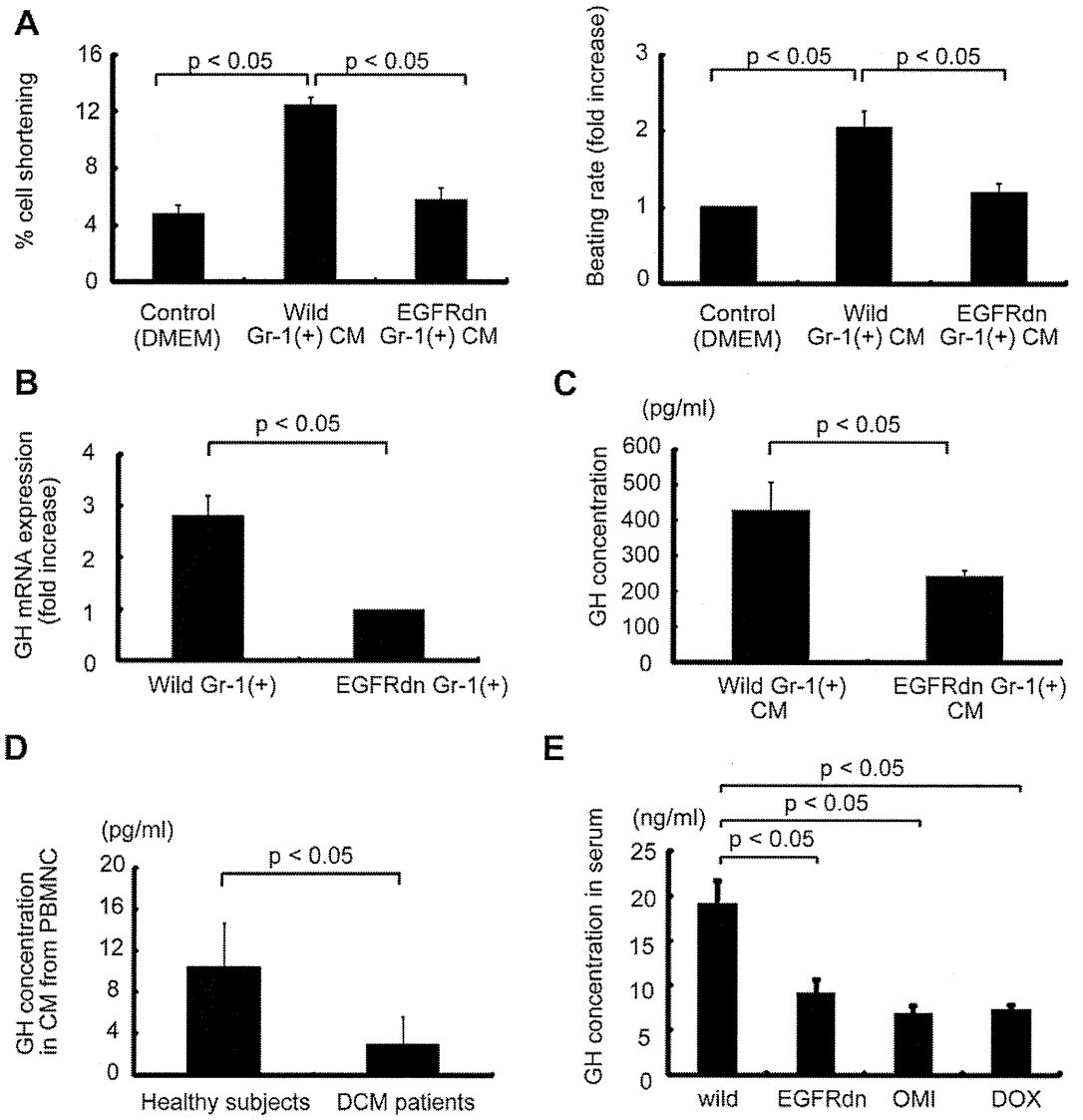

Figure 4. Analysis of secreted factors. (A) CM from Gr-1(+) cells from wild-type mice significantly improved the cell shortening and increased the beating rate in neonatal rat cardiomyocytes, as compared with CM from Gr-1(+) cells from EGFRdn mice. Left graph, cell shortening ($n = 24$ cells per group). Right graph, beating rate ($n = 24$ cells per group). (B) Quantitative RT-PCR analysis of GH mRNA in Gr-1(+) cells isolated from wild-type mice and EGFRdn mice ($n = 4$). (C, D) GH concentrations in (C) CM from Gr-1(+) cells isolated from wild-type mice and EGFRdn mice ($n = 4$) and (D) CM from PBMNC isolated from healthy ($n = 11$) and DCM subjects ($n = 10$). (E) GH concentration in serum from several mouse models of heart failure ($n = 4$). Data are means ± s.e.m.
doi:10.1371/journal.pone.0027901.g004

direct effects of GH in CM from Gr-1(+) cells on cardiomyocytes *in vivo* in transgenic mice overexpressing a dominant-negative mutant of STAT3 (STAT3dn) under the control of an αMHC promoter [13]. The Gr-1(+) cell CM-mediated improvements in cardiac function were not observed in DOX-treated STAT3dn mice (Figure S8), indicating that the CM improves cardiac function through activation of STAT3 in cardiomyocytes.

Upregulation of activin A in heart failure inhibits GH expression in Gr-1(+) cells

The expression of the GH gene has been reported to be regulated by transcription factors including pituitary transcription activator-1 (pit-1) [14], [15], and activin A has been reported to downregulate GH expression by reducing the stability of pit-1 [16]. Since activin A in the peripheral blood of heart failure patients has been reported to be upregulated compared with that in healthy controls [17], we investigated the role of activin A in the downregulation of GH in Gr-1(+) cells. Serum activin A levels were significantly higher in EGFRdn mice than in wild-type mice (Figure 6A), and were also elevated in other murine models of heart failure, including the OMI and DOX models (Figure S9). When Gr-1(+) cells were cultured with 400 pg/ml of activin A, a concentration equivalent to that in the peripheral blood of DCM mice, mRNA and protein levels of GH were significantly downregulated (Figure 6B), suggesting that activin A might be a key mediator of the reduced expression of GH in the Gr-1(+) cells of DCM mice. Furthermore, the serum activin A levels were remarkably higher in DCM patients (Table S1) than in healthy subjects (Figure 6A), while the GH levels in CM from peripheral blood mononuclear cells (PBMNC) of DCM patients was lower than that in healthy subjects (Figure 4D), suggesting that the

Table 1. DNA microarray analysis.

The fold increase	Gene symbol
4.9	Gh
4.3	Pdgfd
3.9	Figf
3.4	Tslp
3.2	Socs2
3.1	Lta
3.0	Bmp1
2.9	Il33
2.8	Ccl27a
2.7	Fgf20
2.6	Angpt1
2.5	Cxcl9
2.4	Il13
2.3	Fam3b
2.3	Il31
2.3	Gm6590
2.2	Spred1
2.2	Cmtm8
2.1	Kitl
2.1	Mif
2.1	Grem2
2.1	Il17d
2.1	Gdf10
2.0	Cxcl5

Each number indicates the fold-increase of gene expression in Gr-1(+) cells isolated from wild-type mice compared with those from EGFRdn mice.
doi:10.1371/journal.pone.0027901.t001

higher activin A levels might also inhibit GH expression in heart failure patients. A recent study showed that PBMNC are a major source of activin A in heart failure [17]. Since many humoral factors are known to contribute to the pathophysiology of heart failure [18], we examined whether humoral factors upregulated in heart failure might regulate activin A expression. Angiotensin II (AngII) (Figure 6C) and tissue necrosis factor-alpha (TNFα) (Figure S10A) increased the activin A levels in CM of PBMNC in a dose-dependent manner. Consistent with the previous reports [19], AngII and TNFα activated NFκB in the PBMNC (Figure 6D and Figure S10B) and AngII- and TNFα-induced upregulation of activin A in PBMNC were inhibited with a NFκB inhibitory peptide (Figure 6E and Figure S10C).

Inhibition of activin A in heart failure increases GH levels and improves cardiac function

To elucidate the role of activin A in EGFRdn mice, anti-activin A antibody was injected intraperitoneally for 2 weeks, with an alternate-day treatment regimen. Inhibition of activin A significantly increased GH protein levels in the CM from Gr-1(+) cells (Figure 6F). Furthermore, when neonatal rat cardiomyocytes were cultured with CM from Gr-1(+) cells isolated from anti-activin A antibody-treated EGFRdn mice, cell shortening was enhanced and the beating rate was increased significantly, as compared with CM from Gr-1(+) cells without antibody treatment (Figure 6G). Consistent with the upregulation of GH levels in Gr-1(+) cells by anti-activin A antibody treatment, the serum GH levels in EGFRdn mice were also increased (Figure 6H). Furthermore, FS and +dp/dt in EGFRdn mice treated with anti-activin A antibody were markedly improved compared with EGFRdn mice treated with isotype control (Figure 6H). Collectively, these results strongly suggest that inhibition of activin A improves cardiac function in non-ischemic DCM mice by restoring GH levels.

Discussion

Functional benefits of BMMNC infusion have been reported in human with ischemic heart diseases [2],[20]. Although we also observed the improvement of cardiac function of DCM model mice by BMMNC infusion, no engraftment of infused BMMNC was observed in the heart. At 3 d after infusion, BMMNC were only observed in the peripheral blood and spleen, but not in the heart, and very few GFP-positive cells were observed at 14 d even in the peripheral blood. This is consistent with the observations that BMMNC infusion only transiently improved cardiac function after infusion. These findings suggest that BMMNC improve cardiac function *via* humoral factors rather than *via* transdifferentiation into cardiomyocytes.

GH plays important roles in the protection of various tissues as well as the growth and development of many organs and whole body [21]. Serum GH levels have been reported to be low in patients with congestive heart failure [22]. Recent animal studies have demonstrated that GH treatment improves cardiac functions [23], [24]. The growth and protection of cardiomyocytes are regulated by various kinases such as Akt, Erk and Jak/Stat, and many studies have demonstrated that activation of Akt and Erk induces cardiac hypertrophy [25], [26] and prevents cardiomyocytes from stress-induced apoptosis [27]. Transgenic mice with cardiac-specific overexpression of the *stat3* gene were reported to show marked ventricular hypertrophy [28], while the cardioprotective effects of several cytokines including granulocyte colony-stimulating factor were reduced in mice with cardiac-specific expression of dominant-negative *stat3* [29]. In this study, we showed that GH produced by Gr-1(+) cells activated Akt, Erk, Jak2, Stat3/5 and PKA, and increased the levels of cAMP in neonatal rat cardiomyocytes (Figure 5C, D). GH has been reported to increase cAMP and activate PKA in reproductive organs by still-unknown mechanisms [30]. Here, we found that the beneficial effects of CM from Gr-1(+) cells on cardiac function were inhibited in cardiac-specific STAT3dn mice, suggesting that GH secreted by Gr-1(+) cells directly affects cardiomyocyte contractility. It has been reported that GH exerts some functions through the induction of IGF-1 expression [31], [32], and IGF-1 also promotes several cardioprotective effects in part by activating the Akt/phosphatidylinositol 3-kinase pathway [33], [34]. In the present study, the specific GH receptor inhibitor, but not anti-IGF-1 antibody, attenuated the improvements of cardiac contractility by the treatment of CM from Gr-1(+) cells in vitro (Figure 5A, B) and in vivo (Figure 5E, F). These findings suggest the effects of Gr-1(+) cells-derived CM on cardiac function of DCM mice mainly depend on GH rather than IGF-1.

It has been reported that the expression of GH gene is regulated by pit-1 at the transcriptional level [14], [15] and that activin A destabilizes pit-1 by phosphorylation [16]. Consistent with a previous report showing higher serum activin A levels in heart failure patients than in healthy controls [17], we found that serum levels of activin A were increased while GH levels in PBMNC CM were decreased in DCM patients. Similarly, the activin A levels were higher in the peripheral blood of DCM mice than in wild-type mice and activin A inhibited the production of GH in Gr-1(+)

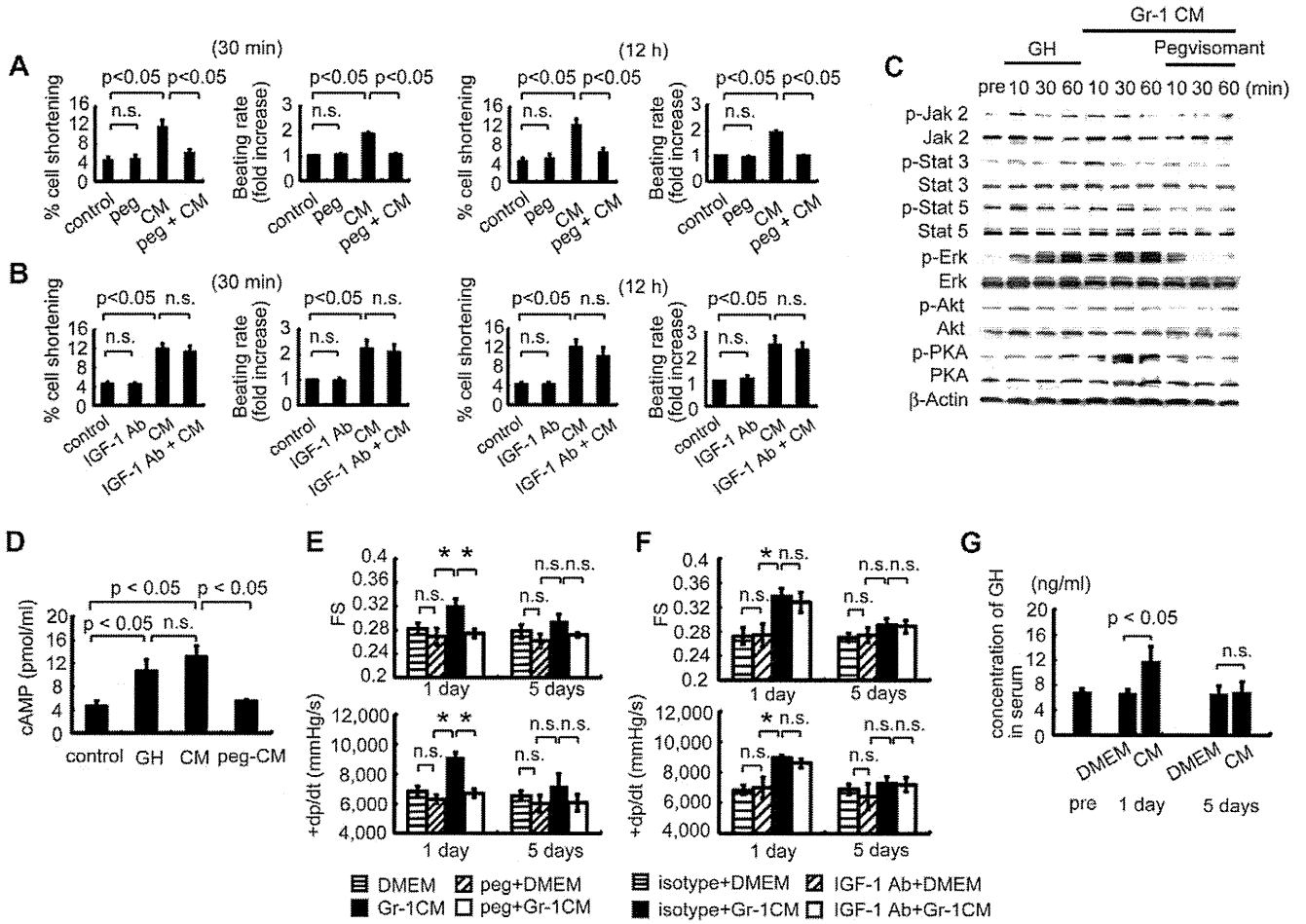

Figure 5. GH mediates the cardioprotective effects of Gr-1(+) cell-derived CM. (A) Pegvisomant (PEG) treatment inhibited the Gr-1(+) cell CM-mediated improvements cardiomyocyte cell shortening and beating rate at 30 min and at 12 h after treatment ($n = 27$ cells per group). Left graphs, cell shortening; right graphs, beating rate. (B) Anti-IGF-1 antibody failed to affect the Gr-1(+) cell CM-mediated improvements in cell shortening or beating rate at 30 min or at 12 h after treatment ($n = 23$ cells per group). Left graphs, cell shortening; right graphs, beating rate. (C) GH and CM from Gr-1(+) cells phosphorylated Akt, Erk, Jak2, Stat3/5 and PKA in cardiomyocytes ($n = 3$), which was inhibited by pegvisomant ($n = 3$). (D) GH (500 pg/ml) and CM from Gr-1(+) cells increased the cAMP concentration in cardiomyocytes ($n = 5$), which was inhibited by pegvisomant ($n = 5$). (E, F) Cardiac function analysis by echocardiography (upper graphs, $n = 8$) and catheterization (lower graphs, $n = 8$). Pegvisomant (E), but not anti-IGF-1 antibody (F), inhibited the improvements in FS and +dp/dt elicited by the infusion of CM from Gr-1(+) cells. *$p<0.05$ ($n = 8$). (G) Serum GH concentrations in DOX mice treated with CM from Gr-1(+) cells ($n = 4$ per group). The infusion of CM from Gr-1(+) cells from wild-type mice increased the serum GH concentration at 1 d, but not at 5 d. Data are means ± s.e.m.

doi:10.1371/journal.pone.0027901.g005

cells *in vitro*. These findings suggest that activin A, which is upregulated in heart failure, inhibits GH expression in various tissues/cells, including BMMNC. Treatment with anti-activin A antibody restored GH levels in Gr-1(+) cells and serum of EGFRdn mice and improved cardiac function, suggesting that normalizing the GH levels by inhibiting activin A is a novel therapeutic strategy for heart failure. Since many humoral factors such as AngII and TNFα are upregulated in heart failure and increased activin A expression by activating NFκB, the molecules that modulate NFκB activation might be also therapeutic targets to restore GH levels. On the other hand, anti-activin A treatment also increased expression levels of GH mRNA in the pituitary (N.F. K.M., unpublished data), suggesting that upregulation of activin A in heart failure might inhibit the expression of GH not only in Gr-1(+) cells but also in the pituitary, and that anti-activin A treatment might improve cardiac function of DCM mice in part by restoring GH expression in the pituitary.

The effects of GH on heart failure have been examined in many animal experiments and clinical trials [35]. A recent meta-analysis revealed that GH treatment improved several clinical parameters including left ventricular end-diastolic dimension, ejection fraction and New York Heart Association functional class [36]. Conversely, non-response to GH treatment for heart failure has been ascribed to GH resistance [37]. In patients with cardiac cachexia, GH levels were reported to be enhanced when compared with non-cachectic patients and normal subjects [38]. In this study, GH levels in heart failure mice and patients were significantly lower than those in healthy control subjects. Moreover, GH derived from Gr-1(+) cells improved cardiac function of heart failure animals, suggesting that our models were in a non-cachectic state and non-cachectic patients of heart failure might be suitable for GH treatment. Because of only temporary improvements in cardiac function (Figure 2A), bone marrow cell infusion might not be an appropriate treatment for heart failure, however inhibition

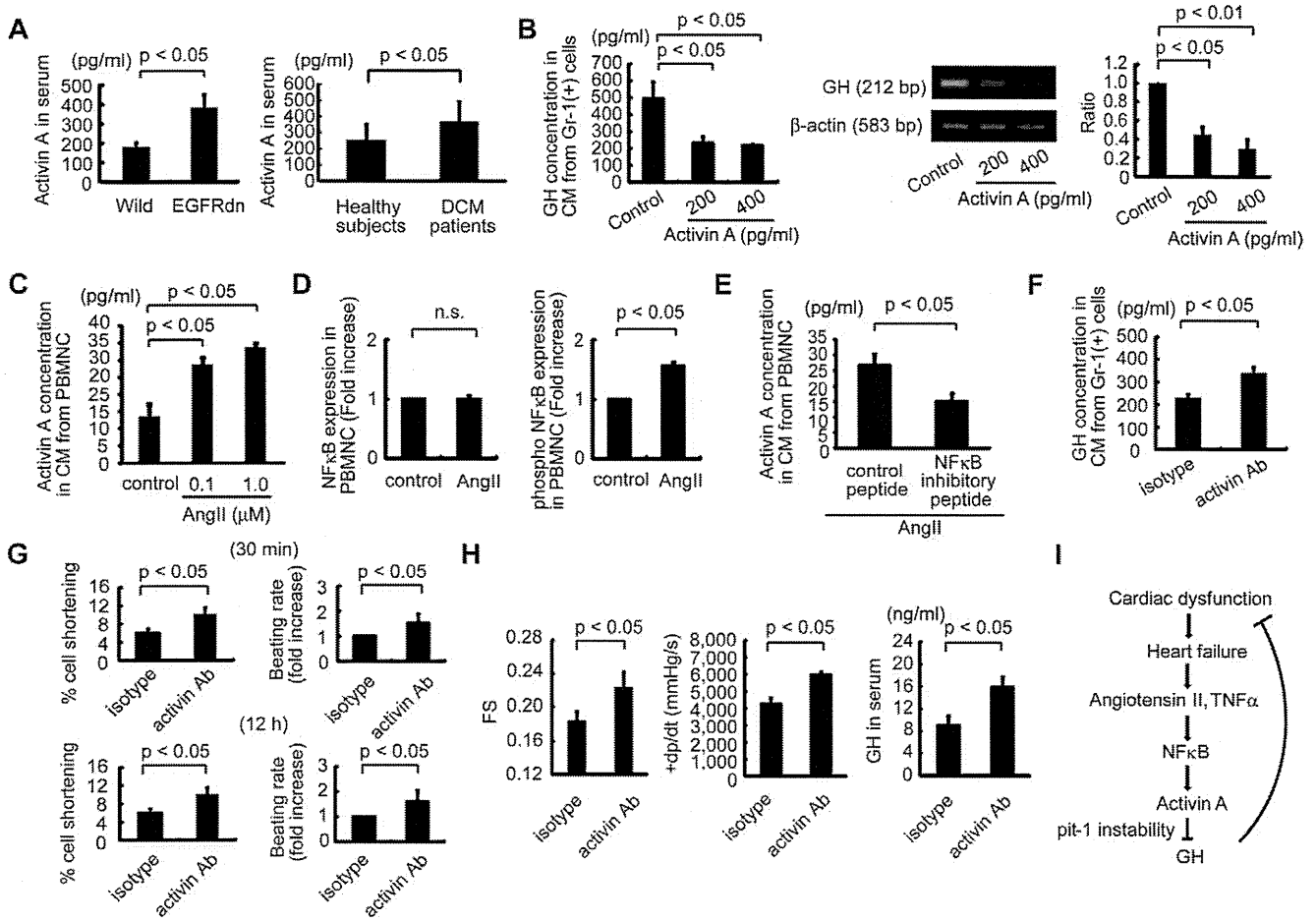

Figure 6. Regulatory mechanisms of GH in heart failure. (A) The serum activin A concentration was higher in EGFRdn mice (left, $n=5$) and in DCM patients (right, $n=10$) than in wild-type mice ($n=5$) and healthy subjects ($n=11$). (B) Activin A downregulated GH mRNA expression in Gr-1(+) cells and GH protein levels in Gr-1(+) cell CM. Left graph, GH protein concentration; middle photographs, representative semi-quantitative RT-PCR images; right graph, GH mRNA expression ($n=3$). (C, D) AngII upregulated activin A secretion (C, $n=4$) and phosphorylated NFκB expression (D, $n=5$) in wild-type PBMNC. (D) Left graph, total NFκB; right graph, phosphorylated NFκB. (E) Inhibition of NFκB [50 μM; NFκB p65 (Ser276) inhibitory peptide] suppressed AngII (10 μM)-mediated upregulation of activin A in CM derived from wild-type PBMNC ($n=5$). Isotype peptide was used as control. (F) The GH concentration in CM from EGFRdn Gr-1(+) cells ($n=5$) was significantly increased by treatment with an anti-activin A antibody ($n=5$). (G) Effects of anti-activin A antibody treatment on cell shortening and the beating rate of cardiomyocytes induced by CM from Gr-1(+) cells isolated from EGFRdn mice ($n=18$ cells per group). (H) Treatment with the anti-activin A antibody improved the cardiac function of EGFRdn mice. Left graph, echocardiography ($n=7$). Middle graph, miller catheter results ($n=7$). Right graph, serum GH concentration in EGFRdn mice after antibody treatment ($n=7$). Data are means ± s.e.m. (I) Proposed mechanism underlying impaired GH expression by activin A in heart failure.
doi:10.1371/journal.pone.0027901.g006

of activin A and enhancement of GH levels might offer novel therapeutic strategies for heart failure.

We used EGFRdn for DCM model mice in this study. It has been reported that cardiac-specific mutant of *ErbB2*, a member of the EGFR/erbB family, shows a severe dilated cardiomyopathy in mice [39]. In the clinical setting, trastuzumab, an anti-cancer agent, is humanized monoclonal antibody that targets the extracellular domain of the human epidermal growth factor receptor 2 and the use of trastuzumab demonstrated an unexpectedly high incidence of both asymptomatic and symptomatic cardiomyopathy. EGFRdn is a compatible DCM model mouse, resembling the cardiotoxic effects observed in patients treated with trastuzumab [40], [41].

There is a limitation in this study. We examined the surface area of neonatal rat cardiomyocytes after the treatment with CM from Gr-1(+) cells or BMMNC as an index for cardiac hypertrophy. However, the surface area not only depends on cell volume, but also on the degree of adhesion and spreading on the culture dishes.

Materials and Methods

Ethics Statement. The ethical committee of Tokyo Women's Medical University reviewed and approved the study protocol (approval ID: 1795). The study was conducted in accordance with the Declaration of Helsinki. We obtained informed consent from the all patients and the all healthy subjects by written before inclusion in this study.

Animals. Wild-type mice (C57BL/6) were purchased from Japan SLC. Adult GFP transgenic mice (C57BL/6) were a kind gift from Dr. M. Okabe (Osaka University). Cardiac-specific dominant-negative STAT3 mice were a kind gift from Dr. K. Yamauchi-Takihara (Osaka University). Neonatal Wistar rats (0–1 d old) were purchased from Saitama Experimental Animals Supply. All protocols were approved by the Institutional Animal Care and Use Committee of Tokyo Women's Medical University and Chiba University. The approval IDs for the animal experiments were 11–34 in Tokyo Women's Medical University

and A21–178 in Chiba University. Doxorubicin (10 mg/kg body weight) was intraperitoneally injected into wild-type male mice (C57BL/6) once-weekly at weeks 7 and 8 after birth. After both Doxorubicin injections, the mice were reared for a further 2 weeks, and the surviving mice were used for experiments. Myocardial infarction models were prepared using wild-type male mice (C57BL/6) as previously described [11]. Serum and Gr-1(+) cells were isolated 4 weeks after inducing myocardial infarction (11 weeks of age).

Generation of EGFRdn mice. The C-terminal 533 amino acids [42] were deleted from the full-length human *EGFR* cDNA (a gift from Professor T. Kadowaki, The University of Tokyo) by introducing a stop codon (TGA) after the R677 codon by site-directed mutagenesis. The truncated *EGFR* (*EGFRdn*) cDNA was then subcloned into the *αMHC* promoter-containing expression vector (a gift from Professor J. Robbins, Cincinnati Children's Hospital). The 8.2-kb DNA fragment was microinjected as a transgene into pronuclei of eggs from BDF1 mice. The eggs were then transferred into the oviducts of pseudopregnant ICR mice. The transgenic founders were identified by Southern blot and PCR analysis. Line 2–5 and Line 9–12 were established and maintained by breeding to C57BL/6 mice. Line 9–12 was selected for further analysis on the basis of a higher level of transgene expression.

BMMNC infusion and CM injection. BMMNC (2.0×10^7) isolated from a male wild-type mouse and suspended in 200 μl of PBS or an equal volume of PBS as a control were injected into the tail veins of anesthetized (4% inhaled isoflurane) 8-week-old male EGFRdn mice and 11-week-old male DOX and OMI mice. CM (200 μl) from Gr-1(+) cells from male wild-type mice or isovolume serum-depleted DMEM were infused into the tail veins of anesthetized 8-week-old male EGFRdn mice and 11-week-old male DOX mice under anesthesia. Anti-mouse insulin-like growth factor-1 (IGF-1) (0.1 μg/g body weight) or anti-goat immunoglobulin G (IgG) (0.1 μg/g body weight) antibodies were intraperitoneally injected into 11-week-old male DOX mice 2 h before CM infusion. Anti-activin A (20 μg) or anti-mouse IgG (20 μg) antibodies were intraperitoneally injected at 48-h intervals into male EGFRdn mice from 10 to 12 weeks of age. Pegvisomant (10 mg/kg body weight) or vehicle (control) were intraperitoneally injected into 8-week-old male DOX mice 30 min before CM infusion.

Evaluation of cell shortening and the beating rate of cardiomyocytes. After 12 h starvation with 500 μl serum-depleted DMEM in 12-well dishes, rat cardiomyocytes were cultured with 500 μl of CM or serum-depleted DMEM. At specific times, the cultured cardiomyocytes were video recorded for 10 sec, and the percentage of cell shortening was analyzed using ImageExpress version 5.5 (Nippon Roper). To measure the percentage of cell shortening, two regions of interest were fixed by the software, which analyzed the beating distance of a single cardiomyocyte, and divided the distance by the length between the regions of interest. The number of beats of single cardiomyocyte was counted for 10 sec to determine the beating rate. For antibody treatment *in vitro*, the starved cardiomyocytes were pretreated with anti-IGF-1 (10 μg/ml) or anti-goat IgG (10 μg/ml) antibodies for 2 h before adding CM. For pegvisomant treatment *in vitro*, the cardiomyocytes were pretreated with pegvisomant (12.5 μg/ml) for 30 min before adding CM.

Echocardiography and catheterization. Transthoracic echocardiographic analysis and catheterization analysis were performed as previously described [11]_ENREF_9. Briefly, the +dp/dt in the left ventricle was measured using a catheter, which was introduced retrogradely *via* the carotid artery.

Cell isolation. Neonatal rat cardiomyocytes were isolated and separately collected as described previously [43]. Cardiomyocytes were plated at a density of 1×10^5 cells/cm^2 on six-, 12- and 24-well dishes (BD Falcon) coated with 1% gelatin and cultured in DMEM supplemented with 10% FBS. Adult cardiomyocytes were prepared as previously described [44]. BMMNC and PBMNC were isolated from 8-week-old male C57BL/6, male GFP mice, and male EGFRdn mice by density gradient centrifugation with Histopaque-1083, as previously described [45]. PBMNC were also isolated from human subjects, as previously described [46].

Sorting of harvested BMMNC into sub-populations and collection of CM. After BMMNC were harvested from male wild-type mice, the cells were sorted into Gr-1(+) cells, B220(+) cells, TER(+) cells, and lineage-negative populations using a Magnetic Cell Sorting system (Miltenyi Biotec), as previously described [47]. To collect the CM, the individual sub-populations were seeded onto 24-well dishes with 200 μl of serum-depleted DMEM. After incubation for 24 h in serum-depleted DMEM, the supernatant (CM) was collected, and any cells were removed by filtering through a 0.45-μm filter (BD Falcon).

Phase-contrast live imaging. Live images of beating cardiomyocytes were taken using a Leica inverted microscope (Leica) equipped with a phase-contrast objective and a CCD camera (Leica).

Flow cytometry. The percentage of cells expressing each cell surface antigen was analyzed using a FACSCalibur (Becton Dickinson Immunocytometry Systems) and Cell Quest Pro version 5.2 software.

RNA extraction and DNA microarray analysis. Total RNA was extracted from 12-week-old male wild-type ($n=4$) and age-matched male EGFRdn mice ($n=4$) using a RNeasy Mini Kit (Qiagen) according to the manufacturer's protocol. RNA quality was assessed with an Agilent 2100 Bioanalyzer (Agilent Technologies). cRNA preparation, fragmentation, hybridization, and scanning of a GeneChip® Mouse Genome 430 2.0 Arrays (Affymetrix) were performed according to the manufacturer's protocol. cRNA was labeled using a Two-cycle Eukaryotic Target Labeling assay with a GeneChip Expression 3′ amplification two-cycle labeling and control reagents kit (Affymetrix). Briefly, cDNA was generated from total RNA (100 ng) using SuperScript II (Invitrogen) and a T7-oligo(dT) promoter primer (Affymetrix). After second-strand cDNA synthesis, cDNA was converted to cRNA by an *in vitro* transcription reaction (MEGAscript T7 kit, Ambion). The cRNA was then purified using a Sample Cleanup Module (Affymetrix), and the yield was monitored with a spectrophotometer. The second cycle of cDNA synthesis was performed, followed by the same cleanup as above and a second *in vitro* transcription reaction cycle with biotin-labeled ribonucleotides and T7 RNA polymerase. The labeled cRNA was purified, using a Sample Cleanup Module and denatured at 94°C before hybridization. The samples were hybridized to GeneChip® Mouse Genome 430 2.0 Arrays at 45°C for 16 h with rotation at 60 rpm. The arrays were then washed, stained with phycoerythrin–streptavidin (Molecular Probes), washed, and scanned with a GeneChip Scanner 3000 7G (Affymetrix). The data were analyzed with GeneSpring version 7.3.1 software (Agilent Technologies).

Reverse transcriptase-PCR. RNA extraction and RT-PCR were performed as previously described [11]. Real-time PCR amplification was performed using an Applied Biosystems 7500 real-time PCR system (Applied Biosystems) with QuantiTect SYBR Green PCR Master Mix (Qiagen). The PCR protocol comprised an initial denaturation step (94°C, 15 sec) followed by 60 cycles of amplification and quantification (55°C for 30 sec and 72°C for 35 sec) and a melting curve program (60–95°C). The

relative mRNA expression level was calculated using the standard curve of GAPDH. All samples were independently analyzed at least three times for each gene. Semi-quantitative RT-PCR of GH was performed using 0.4 μg of total RNA and followed by 40 cycles of the above conditions. The primer sequences were QT00311654 (Qiagen) for GH in real-time PCR, 5′-TCCTG-TGGACAGATCACTGC-3′ and 5′-AATGTAGGCACGCTC-GAACT-3′ for GH in semi-quantitative PCR, QT00309099 (Qiagen) for GAPDH, and 5′-GGACCTGGCTGGCCGGGA-CC-3′ and 5′-GCGGTGCACGATGGAGGGGC-3′ for β-actin. For semi-quantitative RT-PCR, the PCR products were size-fractionated by 2% agarose gel electrophoresis.

Northern blot analysis. For northern blot analysis, total RNA (20 μg) was extracted from hearts using TRIzol Reagent (Invitrogen) and hybridized with a cDNA probe for *EGFRdn*. 18S rRNA ethidium bromide staining was used to quantify RNA loading.

Analysis of phosphorylated ErbB receptor expression. Four-week-old mice were anesthetized by intraperitoneal injection of urethane (2 mg/g body weight) followed by intravenous injection of HB-EGF (0.5 μg/g body weight, R&D Systems), NRG-1β (0.5 μg/g body weight, R&D Systems), or vehicle *via* the inferior vena cava. After 5 min, the hearts were immediately excised and homogenized in a buffer containing 50 mmol/l HEPES (pH 7.5), 137 mmol/l NaCl, 1 mmol/l $MgCl_2$, 1 mmol/l $CaCl_2$, 10 mmol/l Na-pyrophosphate, 2 mmol/l EDTA, 1% NP-40, 10% glycerol, 2 mmol/l Na_3VO_4, 10 mmol/l NaF, and protease inhibitor cocktail (Complete Mini, Roche Applied Science). To analyze the tyrosine phosphorylation of ErbB receptors, equivalent amounts of proteins were subjected to immunoprecipitation with the specific antibodies, fractionated by 6% SDS-PAGE, and immunoblotted with the mouse monoclonal anti-phosphotyrosine antibody 4G10 (Millipore). Horseradish peroxidase-conjugated anti-mouse IgG antibody (GE Healthcare) was used as the secondary antibody, and the bound antibodies were detected using an ECL detection kit (GE Healthcare).

ELISA. Serum and CM concentrations of cAMP, GH and activin A were measured by ELISA (cAMP and activin A, R&D Systems; GH, LINCO Research). To prepare cell lysates for cAMP analysis, cardiomyocytes were seeded (4×10^5 cells/cm) onto six-well dishes coated with 1% gelatin and cultured in DMEM supplemented with 10% FBS. After 5 d, the cells were washed three times with PBS and the medium was changed to serum-depleted DMEM. After incubation for 12 h in the serum-depleted medium, the cells were washed three times with PBS and the medium was replaced with 1 ml of serum-depleted DMEM with CM (1 ml), 2 ml of serum-depleted DMEM with 500 pg/ml GH, 2 ml of serum-depleted DMEM with 12.5 μg/ml pegvisomant, or 1 ml of serum-depleted DMEM plus 1 ml of CM and 12.5 μg/ml pegvisomant. Thirty minutes later, the cardiomyocytes were resuspended in lysis buffer in six-well dish.

To examine the expression of NFκB and phosphorylated NFκB in PBMNC, PBMNC isolated from wild-type male mice were cultured with AngII or TNFα. Thirty minutes later, PBMNC were resuspended in lysis buffer and the expression of NFκB and phosphorylated NFκB were examined using sandwich ELISA kits (Cell Signaling). Some cells were also treated with 50 μM NFκB p65 (Ser276) inhibitory peptide to inhibit NFκB activity.

Western blot analysis. Whole-cell lysates (30–50 μg) were resolved by SDS-PAGE. The separated proteins were transferred to a PVDF membrane (GE Healthcare) and incubated with the primary antibody, followed by an anti-IgG-horseradish peroxidase-conjugated secondary antibody. Proteins were detected using an ECL-Plus kit (GE Healthcare).

Immunohistology. The hearts were fixed with 4% paraformaldehyde and embedded in paraffin, or fixed in 10% neutralized formalin and embedded in Tissue-Tek OCT cryo-embedding compound (Sakura Finetek). The specimens were sectioned (5 μm thick), and stained with hematoxylin/eosin or Masson trichrome.

Evaluation of cardiac hypertrophy. To evaluate the mean diameter of LV cardiomyocytes, the shortest diameter of each cardiomyocyte was measured in nucleated transverse sections stained with hematoxylin-eosin. Thirty cardiomyocytes in each LV were measured using an ocular micrometer disc with a linear scale at a magnification of 400×, and the average cardiomyocyte diameter was calculated for each specimen. Four hearts were measured in each group. The cell surface area of isolated neonatal and adult cardiomyocytes was measured by planimetry in 50 randomly selected cells per specimen.

Immunofluorescence staining. Immunostaining was performed as previously described [45]. Images were taken using a fluorescent microscopy (Leica) with LAS AF software (Leica).

Human subjects. We enrolled 10 subjects who were outpatients of Department of Cardiology of Tokyo Women's Medical University Hospital. We obtained 10 ml of whole blood from each patient. Half of the blood sample was used to measure the serum activin A concentration and the remaining blood was used to measure GH in CM after PBMNC isolation. All patients were receiving medical therapies and exhibited New York Heart Association class II symptoms. We also enrolled 11 healthy age- and body mass index-matched volunteers. Characteristics of the patients and healthy subjects are summarized in Table S1.

Statistics. Data are presented as means ± s.e.m. We examined differences between groups by Student's *t* test or analysis of variance followed by Bonferroni's correction to compare means. A value of $P<0.05$ was considered to be significant.

Supporting Information

Figure S1 Overexpression of EGFRdn inhibited the functional activation of endogenous ErbB receptors in a dominant-negative manner. (A) Northern blot analysis for the transgene expression in hearts from wild-type and two different founder lines of EGFRdn mice (L2–5 and L9–12). (B) Tyrosine phosphorylation of ErbB receptors in hearts from wild-type and EGFRdn mice (L9–12) at 5 min after injection of HB-EGF. In wild-type mice, intravenous injection of HB-EGF enhanced cardiac tyrosine phosphorylation of EGFR, ErbB2 and ErbB4, which was abrogated in EGFRdn hearts. HB-EGF, heparin-binding EGF-like growth factor. (C) Tyrosine phosphorylation of ErbB receptors in hearts from wild-type and EGFRdn mice (L9–12) at 5 min after the injection of NRG-1β. NRG-1β induced tyrosine phosphorylation of ErbB2 and ErbB4 in wild-type hearts, but not in EGFRdn hearts. NRG-1, neuregulin-1.
(TIF)

Figure S2 Echocardiographic analysis of DOX mice. (A) Representative M-mode images of wild-type and DOX mice. (B) Left ventricular diastolic and systolic dimensions, and FS of 11-week-old DOX mice ($n=36$) and age-matched wild-type mice ($n=10$). LVDd, left ventricular diastolic dimension; LVDs, left ventricular systolic dimension. Data are means ± s.e.m.
(TIF)

Figure S3 Analysis of cardiac hypertrophy. (A) The shortest diameter of each cardiomyocyte ($n=30$ per group). Lower photographs, H&E-stained tissue sections. Scale bar, 75 μm. (B) Surface area of isolated adult cardiomyocytes ($n=50$ per group).

Lower photographs, representative images. Scale bar, 75 μm. Data are means ± s.e.m.
(TIF)

Figure S4 Flow cytometric analysis. The left and right panels show the expression of each cell surface marker before and after magnetic sorting (MACS), respectively.
(TIF)

Figure S5 Cardiac hypertrophy *in vitro*. Upper graph, cell surface area of neonatal rat cardiomyocytes ($n = 50$); lower photographs, representative images of the cells. Cardiomyocytes were stained with sarcomeric α-actinin (red). Nuclei were stained with Hoechst 33258 (blue). Scale bars, 75 μm. Data are means ± s.e.m.
(TIF)

Figure S6 Comparison of GH concentration. GH concentration in CM from Gr-1(+) cells isolated from old myocardial infarction (OMI) mice and DOX mice ($n = 5$). Data are means ± s.e.m.
(TIF)

Figure S7 BMMNC improve the cardiac function of OMI mice via the GH receptor. (A) At 4 weeks after coronary ligation, BMMNC were infused via the tail vein. Pegvisomant (10 mg/kg body weight) or vehicle (control) was intraperitoneally injected into OMI mice 30 min before infusing BMMNC. BMMNC infusion improved FS and +dp/dt at 3 d after infusion and these improvements were inhibited by pegvisomant (n = 5). (B) Masson trichrome staining. Panels show representative images. Scale bars: 1 mm. Data are means ± s.e.m.
(TIF)

Figure S8 Direct effects of GH in the CM from Gr-1(+) cells on cardiomyocytes. CM from Gr-1(+) cells from wild-type mice was infused into DOX-treated wild-type mice (wild-DOX) or DOX-treated cardiac-specific STAT3dn mice (STAT3dn-DOX). Gr-1(+) cell-derived CM improved FS (left) and +dp/dt (right) in wild-DOX mice ($n = 5$) at 1 d after infusion, but not in STAT3dn-DOX ($n = 5$). Data are means ± s.e.m.
(TIF)

Figure S9 Serum activin A concentrations ($n = 5$). Data are means ± s.e.m.
(TIF)

Figure S10 TNFα increases the secretion of activin A from PBMNC *via* NFκB. (A) Activin A levels in CM from PBMNC were upregulated by treatment with TNFα ($n = 5$). (B) TNFα (50 ng/ml) activated NFκB in PBMNC ($n = 5$). Left, total NFκB; right, phosphorylated NFκB. (C) TNFα (50 ng/ml) -mediated upregulation of activin A in PBMNC was inhibited by treatment with the NFκB inhibitory peptide ($n = 5$). Isotype peptide was used as control. Data are means ± s.e.m.
(TIF)

Table S1 Characteristics of human subjects.
(PDF)

Acknowledgments

We thank M. Okabe (Osaka University, Japan) for the GFP transgenic mice, K. Yamauchi-Takihara (Osaka University) for the cardiac-specific STAT3dn mice, N. Ueno (Tokyo Women's Medical University) for manuscript preparation, T. Kadowaki (The University of Tokyo, Tokyo), J. Robbins (Children's Hospital, Cincinnati, OH) for providing cDNAs, A. Suzuki and K. Nomura (Tokyo Women's Medical University) for their technical supports, and H. Nagao and K. Yoshihara for their excellent technical assistance.

Author Contributions

Conceived and designed the experiments: KM IK. Performed the experiments: NF KM HA AH TN TT AS KMM. Analyzed the data: NF KM HA. Contributed reagents/materials/analysis tools: TS TO. Wrote the paper: NF KM NH IK.

References

1. Passier R, van Laake LW, Mummery CL (2008) Stem-cell-based therapy and lessons from the heart. Nature 453: 322–329.
2. Schachinger V, Erbs S, Elsasser A, Haberbosch W, Hambrecht R, et al. (2006) Intracoronary bone marrow-derived progenitor cells in acute myocardial infarction. N Engl J Med 355: 1210–1221.
3. Segers VF, Lee RT (2008) Stem-cell therapy for cardiac disease. Nature 451: 937–942.
4. van Ramshorst J, Bax JJ, Beeres SL, Dibbets-Schneider P, Roes SD, et al. (2009) Intramyocardial bone marrow cell injection for chronic myocardial ischemia: a randomized controlled trial. JAMA 301: 1997–2004.
5. Martin-Rendon E, Brunskill SJ, Hyde CJ, Stanworth SJ, Mathur A, et al. (2008) Autologous bone marrow stem cells to treat acute myocardial infarction: a systematic review. Eur Heart J 29: 1807–1818.
6. Donndorf P, Kundt G, Kaminski A, Yerebakan C, Liebold A, et al. (2011) Intramyocardial bone marrow stem cell transplantation during coronary artery bypass surgery: A meta-analysis. J Thorac Cardiovasc Surg.
7. Orlic D, Kajstura J, Chimenti S, Jakoniuk I, Anderson SM, et al. (2001) Bone marrow cells regenerate infarcted myocardium. Nature 410: 701–705.
8. Murry CE, Soonpaa MH, Reinecke H, Nakajima H, Nakajima HO, et al. (2004) Haematopoietic stem cells do not transdifferentiate into cardiac myocytes in myocardial infarcts. Nature 428: 664–668.
9. Cho HJ, Lee N, Lee JY, Choi YJ, Ii M, et al. (2007) Role of host tissues for sustained humoral effects after endothelial progenitor cell transplantation into the ischemic heart. J Exp Med 204: 3257–3269.
10. Gnecchi M, He H, Liang OD, Melo LG, Morello F, et al. (2005) Paracrine action accounts for marked protection of ischemic heart by Akt-modified mesenchymal stem cells. Nat Med 11: 367–368.
11. Matsuura K, Honda A, Nagai T, Fukushima N, Iwanaga K, et al. (2009) Transplantation of cardiac progenitor cells ameliorates cardiac dysfunction after myocardial infarction in mice. J Clin Invest 119: 2204–2217.
12. Muller AF, Kopchick JJ, Flyvbjerg A, van der Lely AJ (2004) Clinical review 166: Growth hormone receptor antagonists. J Clin Endocrinol Metab 89: 1503–1511.
13. Funamoto M, Fujio Y, Kunisada K, Negoro S, Tone E, et al. (2000) Signal transducer and activator of transcription 3 is required for glycoprotein 130-mediated induction of vascular endothelial growth factor in cardiac myocytes. J Biol Chem 275: 10561–10566.
14. Bodner M, Castrillo JL, Theill LE, Deerinck T, Ellisman M, et al. (1988) The pituitary-specific transcription factor GHF-1 is a homeobox-containing protein. Cell 55: 505–518.
15. Ingraham HA, Chen RP, Mangalam HJ, Elsholtz HP, Flynn SE, et al. (1988) A tissue-specific transcription factor containing a homeodomain specifies a pituitary phenotype. Cell 55: 519–529.
16. Gaddy-Kurten D, Vale WW (1995) Activin increases phosphorylation and decreases stability of the transcription factor Pit-1 in MtTW15 somatotrope cells. J Biol Chem 270: 28733–28739.
17. Yndestad A, Ueland T, Oie E, Florholmen G, Halvorsen B, et al. (2004) Elevated levels of activin A in heart failure: potential role in myocardial remodeling. Circulation 109: 1379–1385.
18. Schrier RW, Abraham WT (1999) Hormones and hemodynamics in heart failure. N Engl J Med 341: 577–585.
19. Takahashi M, Suzuki E, Takeda R, Oba S, Nishimatsu H, et al. (2008) Angiotensin II and tumor necrosis factor-alpha synergistically promote monocyte chemoattractant protein-1 expression: roles of NF-kappaB, p38, and reactive oxygen species. Am J Physiol Heart Circ Physiol 294: H2879–2888.
20. Gao LR, Wang ZG, Zhu ZM, Fei YX, He S, et al. (2006) Effect of intracoronary transplantation of autologous bone marrow-derived mononuclear cells on outcomes of patients with refractory chronic heart failure secondary to ischemic cardiomyopathy. Am J Cardiol 98: 597–602.
21. Bartke A (2005) Minireview: role of the growth hormone/insulin-like growth factor system in mammalian aging. Endocrinology 146: 3718–3723.
22. Giustina A, Lorusso R, Borghetti V, Bugari G, Misitano V, et al. (1996) Impaired spontaneous growth hormone secretion in severe dialated cardiomyopathy. Am Heart J 131: 620–622.
23. Colligan PB, Brown-Borg HM, Duan J, Ren BH, Ren J (2002) Cardiac contractile function is enhanced in isolated ventricular myocytes from growth hormone transgenic mice. J Endocrinol 173: 257–264.
24. Tajima M, Weinberg EO, Bartunek J, Jin H, Yang R, et al. (1999) Treatment with growth hormone enhances contractile reserve and intracellular calcium

transients in myocytes from rats with postinfarction heart failure. Circulation 99: 127–134.
25. Bueno OF, De Windt LJ, Tymitz KM, Witt SA, Kimball TR, et al. (2000) The MEK1-ERK1/2 signaling pathway promotes compensated cardiac hypertrophy in transgenic mice. EMBO J 19: 6341–6350.
26. Shiojima I, Sato K, Izumiya Y, Schiekofer S, Ito M, et al. (2005) Disruption of coordinated cardiac hypertrophy and angiogenesis contributes to the transition to heart failure. J Clin Invest 115: 2108–2118.
27. Matsui T, Li L, del Monte F, Fukui Y, Franke TF, et al. (1999) Adenoviral gene transfer of activated phosphatidylinositol 3′-kinase and Akt inhibits apoptosis of hypoxic cardiomyocytes in vitro. Circulation 100: 2373–2379.
28. Kunisada K, Negoro S, Tone E, Funamoto M, Osugi T, et al. (2000) Signal transducer and activator of transcription 3 in the heart transduces not only a hypertrophic signal but a protective signal against doxorubicin-induced cardiomyopathy. Proc Natl Acad Sci U S A 97: 315–319.
29. Harada M, Qin Y, Takano H, Minamino T, Zou Y, et al. (2005) G-CSF prevents cardiac remodeling after myocardial infarction by activating the Jak-Stat pathway in cardiomyocytes. Nat Med 11: 305–311.
30. Sirotkin AV (2005) Control of reproductive processes by growth hormone: extra- and intracellular mechanisms. Vet J 170: 307–317.
31. Colao A, Vitale G, Pivonello R, Ciccarelli A, Di Somma C, et al. (2004) The heart: an end-organ of GH action. Eur J Endocrinol 151: S93–101.
32. Colao A (2008) The GH-IGF-I axis and the cardiovascular system: clinical implications. Clin Endocrinol 69: 347–358.
33. Welch S, Plank D, Witt S, Glascock B, Schaefer E, et al. (2002) Cardiac-specific IGF-1 expression attenuates dilated cardiomyopathy in tropomodulin-overexpressing transgenic mice. Circ Res 90: 641–648.
34. Torella D, Rota M, Nurzynska D, Musso E, Monsen A, et al. (2004) Cardiac stem cell and myocyte aging, heart failure, and insulin-like growth factor-1 overexpression. Circ Res 94: 514–524.
35. Marleau S, Mulumba M, Lamontagne D, Ong H (2006) Cardiac and peripheral actions of growth hormone and its releasing peptides: relevance for the treatment of cardiomyopathies. Cardiovasc Res 69: 26–35.
36. Le Corvoisier P, Hittinger L, Chanson P, Montagne O, Macquin-Mavier I, et al. (2007) Cardiac effects of growth hormone treatment in chronic heart failure: A meta-analysis. J Clin Endocrinol Metab 92: 180–185.
37. Cicoira M, Kalra PR, Anker SD (2003) Growth hormone resistance in chronic heart failure and its therapeutic implications. J Card Fail 9: 219–226.
38. Anker SD, Chua TP, Ponikowski P, Harrington D, Swan JW, et al. (1997) Hormonal changes and catabolic/anabolic imbalance in chronic heart failure and their importance for cardiac cachexia. Circulation 96: 526–534.
39. Ozcelik C, Erdmann B, Pilz B, Wettschureck N, Britsch S, et al. (2002) Conditional mutation of the ErbB2 (HER2) receptor in cardiomyocytes leads to dilated cardiomyopathy. Proc Natl Acad Sci U S A 99: 8880–8885.
40. Seidman A, Hudis C, Pierri MK, Shak S, Paton V, et al. (2002) Cardiac dysfunction in the trastuzumab clinical trials experience. J Clin Oncol 20: 1215–1221.
41. Perez EA, Rodeheffer R (2004) Clinical cardiac tolerability of trastuzumab. J Clin Oncol 22: 322–329.
42. Redemann N, Holzmann B, von Ruden T, Wagner EF, Schlessinger J, et al. (1992) Anti-oncogenic activity of signalling-defective epidermal growth factor receptor mutants. Mol Cell Biol 12: 491–498.
43. Ikeda K, Tojo K, Tokudome G, Hosoya T, Harada M, et al. (2000) The effects of sarpogrelate on cardiomyocyte hypertrophy. Life Sci 67: 2991–2996.
44. Zou Y, Akazawa H, Qin Y, Sano M, Takano H, et al. (2004) Mechanical stress activates angiotensin II type 1 receptor without the involvement of angiotensin II. Nat Cell Biol 6: 499–506.
45. Matsuura K, Wada H, Nagai T, Iijima Y, Minamino T, et al. (2004) Cardiomyocytes fuse with surrounding noncardiomyocytes and reenter the cell cycle. J Cell Biol 167: 351–363.
46. Honda A, Matsuura K, Fukushima N, Tsurumi Y, Kasanuki H, et al. (2009) Telmisartan induces proliferation of human endothelial progenitor cells via PPARgamma-dependent PI3K/Akt pathway. Atherosclerosis 205: 376–384.
47. Matsuura K, Nagai T, Nishigaki N, Oyama T, Nishi J, et al. (2004) Adult cardiac Sca-1-positive cells differentiate into beating cardiomyocytes. J Biol Chem 279: 11384–11391.

Advance Publication
Journal of Atherosclerosis and Thrombosis
Vol. 18, No. 12
Accepted for publication: September 6, 2011
Published online: November 10, 2011

Original Article

Patients with CD36 Deficiency Are Associated with Enhanced Atherosclerotic Cardiovascular Diseases

Miyako Yuasa-Kawase[1], Daisaku Masuda[1], Taiji Yamashita[1], Ryota Kawase[1], Hajime Nakaoka[1], Miwako Inagaki[1], Kazuhiro Nakatani[1], Kazumi Tsubakio-Yamamoto[1], Tohru Ohama[1,3], Akifumi Matsuyama[2], Makoto Nishida[1,3], Masato Ishigami[4], Toshiharu Kawamoto[5], Issei Komuro[1] and Shizuya Yamashita[1]

[1]Department of Cardiovascular Medicine, Osaka University Graduate School of Medicine, Osaka, Japan
[2]Department of Somatic Stem Cell Therapy, Institute of Biomedical Research and Innovation, Foundation for Biomedical Research and Innovation, TRI305, Hyogo, Japan
[3]Health Care Center, Osaka University, Osaka, Japan
[4]Department of Biomedical Informatics, Division of Health Sciences, Osaka University Graduate School of Medicine, Osaka, Japan
[5]Kure Heart Center, National Hospital Organization Kure Medical Center, Hiroshima, Japan

Aim: The clustering of dyslipidemia, impaired glucose tolerance and hypertension increases the morbidity and mortality from cardiovascular events. A class B scavenger receptor, CD36, is a receptor for oxidized LDL and a transporter of long-chain fatty acids. Because of the impaired uptake of oxidized LDL in CD36-deficient macrophages and from the results of CD36 knockout mice, CD36 deficiency (CD36-D) was supposed to be associated with reduced risks for coronary artery disease (CAD); however, CD36-D patients are often accompanied by a clustering of coronary risk factors. The current study aimed to investigate the morbidity and severity of cardiovascular diseases in CD36-D patients.
Methods: By screening for CD36 antigen on platelets and monocytes using FACS or the absent myocardial accumulation of ^{123}I-BMIPP by scintigraphy, 40 patients with type I CD36-D were collected, the morbidity of CAD and their features of atherosclerotic cardiovascular diseases were observed. Screening for CD36-D in both CAD patients (n=319) and healthy subjects (n=1,239) were underwent.
Results: The morbidity of CAD was significantly higher in CD36-D patients than in the general population; 50% of patients (20 out of 40) had CAD identified by BMIPP scintigraphy and 37.5% (3 out of 8) by FACS screening, respectively. Three representative CD36-D cases demonstrated severe CAD and atherosclerosis. The frequency of CD36-D was three times higher in CAD patients than in healthy subjects (0.9% vs 0.3%, $p<0.0001$).
Conclusion: The morbidity of CAD is significantly higher in CD36-D patients suffering from severe atherosclerosis, implying that the status of CD36-D might be atherogenic.

J Atheroscler Thromb, 2011; 18:000-000.

Key words; CD36 deficiency, Long-chain fatty acid transporter, Atherosclerotic cardiovascular disease, Insulin resistance, Metabolic syndrome

Introduction

Patients with metabolic syndrome (MetS) are characterized by a clustering of coronary risk factors, such as dyslipidemia including hypertriglyceridemia and a low level of high density lipoprotein-cholesterol (HDL-C), impaired glucose tolerance and hypertension along with the accumulation of abdominal visceral fat. The morbidity and mortality of atherosclerotic cardiovascular events are significantly high in patients with MetS, and the reduction of abdominal visceral fat by diet and exercise therapy is very important for treatment of the clustering of these coronary risk fac-

Address for correspondence: Shizuya Yamashita, MD, PhD, FAHA, FJCC, Department of Cardiovascular Medicine, Osaka University Graduate School of Medicine, 2-2 Yamadaoka, Suita, Osaka 565-0871, Japan
E-mail: shizu@imed2.med.osaka-u.ac.jp
Received: June 13, 2011
Accepted for publication: September 6, 2011

Advance Publication
Journal of Atherosclerosis and Thrombosis
Accepted for publication: September 6, 2011
Published online: November 10, 2011

tors and atherosclerotic cardiovascular diseases.

CD36 is an 88-kDa membrane glycoprotein belonging to a class B scavenger receptor[1]. CD36 is expressed in a variety of cells and tissues including platelets, monocyte/macrophages, heart, skeletal muscle, adipose tissue and small intestines[1]. CD36 is a receptor for oxidized low density lipoproteins (LDL)[2] and a transporter of long-chain fatty acids (LCFA)[3]. CD36-deficient patients were first identified from subjects who were refractory to platelet transfusion[4]. Kashiwagi *et al.* identified several genetic mutations of human CD36 deficiency (CD36-D)[5]. We previously investigated the metabolic phenotypes of CD36-D patients[6-7] and reported that they (high fasting serum triglycerides level, low HDL-C level, fasting hyperglycemia, insulin resistance and hypertension) were frequently observed and clustered in patients with CD36-D, similar to those with MetS[8-9]. It was later reported that the accumulation of these metabolic phenotypes is not due to the deposition of abdominal visceral fat, but to insulin resistance or impaired metabolism of lipoproteins and free fatty acids (FFA) in the postprandial state in patients with CD36-D[8-10]. It is well known that these metabolic profiles are independent coronary risk factors in the general population[11-13]; therefore, the status of human CD36-D was supposed to be atherogenic and the morbidity of atherosclerotic cardiovascular diseases might be high in patients with CD36-D.

In contrast, the status of human CD36-D was supposed to be anti-atherogenic since CD36 is a scavenger receptor for oxidized LDL when the foam cell formation of CD36-D macrophages by exposure of oxidized LDL is impaired[14]. Nozaki et al. showed that the uptake of oxidized LDL was reduced by approximately 40% in macrophages from patients with CD36-D compared with normal controls[15]. Janabi *et al.* showed that the responses of oxidized LDL-induced NF-kappa B activation and subsequent cytokine expression were impaired in monocyte-derived macrophages from CD36-D patients[16]. Furthermore, there have been two reports by Febbraio *et al.* and Moore *et al.* concerning the atherogenicity of genetic disruption of CD36 in mice[17-18]. Both reports showed that macrophage foam cell formation when treated with oxidized LDL was impaired when they crossed CD36 null mice with atherogenic apoE-null mice; however, atherosclerotic lesion development in CD36-apoE double knockout mice was different in these two reports. Febbraio *et al.* showed a 76.5% decrease in aortic tree lesion areas when mice were fed a Western diet and a 45% decrease in the aortic sinus lesion area when fed a normal diet in CD36-apoE double knockout mice, respectively, compared with wild-type mice[17]. In contrast, Moore et al. showed that CD36-apoE double knockout (DKO) mice did not show amelioration of the progression of atherosclerotic lesions but foam cell accumulation at aortic sinus rather increased and the severity of atherosclerotic lesions was advanced in DKO mice compared with apoE-KO mice[18]. From these controversial results, the atherogenicity of CD36-D, especially that of human CD36-D patients, remains unclear.

We have so far identified 40 patients with CD36-D by myocardial scintigraphy using an analogue of LCFA, ^{123}I-BMIPP, or by screening with immunofluorescent flow cytometric analysis (FACS). We experienced three typical cases of severe atherosclerotic cardiovascular diseases in patients with CD36-D who were identified in our previous study[9] and evaluated by imaging studies. In the current study, in order to elucidate whether the morbidity and severity of atherosclerotic cardiovascular diseases are high in patients with CD36-D, we evaluated the prevalence of atherosclerotic cardiovascular diseases in 40 patients with CD36-D. Furthermore, to exclude the patient collection bias and to extend the knowledge to the general population, we compared the prevalence of CD36-D between patients with CAD and healthy subjects. We demonstrate that the morbidity of CAD is significantly higher in CD36-D patients suffering from severe atherosclerosis, implying that the status of human CD36-D might be atherogenic.

Subjects and Methods

Diagnosis of CD36 Deficiency

In our previous study, 40 patients without myocardial accumulation of an LCFA analogue, ^{123}I-beta-methyl-p-iodophenyl-pentadecanoic acid (^{123}I-BMIPP), were identified among patients whose heart was evaluated by single photon emission computed tomography (SPECT) for the evaluation of cardiac performance screening at Osaka University Hospital and related hospitals[9]. In order to confirm the diagnosis of CD36-D in these patients, immunofluorescent flow cytometric analysis was performed by using mouse monoclonal antibodies against CD36 (OKM5; Ortho Diagnostic System Inc., Raritan, NJ) at the Department of Blood Transfusion, Osaka University Hospital[7]. Briefly, 20 ml of blood was drawn, anticoagulated with heparin (10 U/ml), layered over 10 ml Ficoll-Paque (GE Healthcare UK Ltd., Buckinghamshire, UK) and centrifuged at 1,000 g for 30 minutes. A 50 μl suspension of platelets ($2 \times 10^5/\mu$l) or mononuclear cells ($2 \times 10^4/\mu$l) was incubated with FITC-conjugat-

Advance Publication
Journal of Atherosclerosis and Thrombosis
Accepted for publication: September 6, 2011
Published online: November 10, 2011

ed anti-human CD36 monoclonal antibody OKM5 (Ortho Diagnostic Systems) (final concentration: 2.5 μg/ml) or FITC-conjugated mouse IgG (final concentration: 2.5 μg/ml) for 30 minutes at 40℃ and assayed on a FACScan® system (Becton Dickinson Co., Mountain View, CA) as previously reported[7]. Appropriate cell fractions for the analysis of monocytes were selected by a gating method with a two-dimensional display of forward scatter and side scatter of analyzed cells[15]. We diagnosed patients with type I CD36-D whose CD36 antigen was not detected in either monocytes or platelets. Each subject gave written informed consent before participating in the study, and the ethics committee of Osaka University Hospital approved the study design.

Analysis of Clinical Profile and Atherosclerotic Cardiovascular Diseases in Patients with CD36-D

The presence or absence of atherosclerotic cardiovascular diseases was extensively investigated in patients with CD36-D based upon their medical history and symptoms. We assessed the severity of atherosclerotic cardiovascular diseases and risk factors of these patients. Blood pressure was determined in the sitting position, and peripheral venous blood was drawn in the fasting state after overnight fasting and centrifuged for serum separation. Serum levels of total cholesterol (TC), triglycerides (TG), and HDL-cholesterol (HDL-C) as well as fasting plasma glucose levels were measured by enzymatic methods as reported in our previous study[9]. HbA1c was measured by HPLC (Sekisui Medical Co., Tokyo, Japan). All samples were treated in accordance with the Helsinki Declaration. In some patients with CD36-D, coronary angiography was performed for an extensive evaluation of coronary artery atherosclerosis. In order to evaluate atherosclerotic lesions in arteries other than coronary arteries in detail, the thoracic and abdominal aorta and their branches were examined by aortic angiography or magnetic resonance angiography.

Prevalence of CAD in Patients with CD36-D Identified by Absence of Cardiac Uptake of ^{123}I-BMIPP

In order to assess whether patients with CD36-D had a higher mortality and severity of CAD, we evaluated the morbidity of CAD in these patients by checking medical records. The diagnosis of CAD was established when a patient had coronary artery stenosis (≥ 75%) assessed by coronary angiography. The CAD patients were divided into 3 groups by their clinical course and results of coronary angiography: 1) acute or old myocardial infarction, 2) unstable angina, and 3) stable angina.

Prevalence of CAD in Patients with CD36-D Identified by Screening of CD36-D by FACS Analysis in the General Population

For the screening study of CD36-D by FACS analysis, normal healthy volunteers were recruited for over ten years in our laboratory and we found 8 patients with type I CD36-D. We traced their medical records, especially the result of coronary angiography, in order to confirm whether they were accompanied by CAD.

Prevalence of CD36-D in Patients with CAD and Healthy Subjects

In order to evaluate whether the frequency of CD36-D in patients with CAD is higher than in normal healthy subjects, we performed screening examinations in patients with CAD and healthy subjects. Patients with coronary artery stenoses (≥ 75%) were diagnosed with CAD by coronary angiography (n=319). Normal healthy volunteers were recruited using the following criteria: no ST-T abnormalities in ECG, no chest symptoms on effort and no significant coronary artery stenosis (≥ 75%) if they received coronary angiography (n=1,239). Their cell surface CD36 antigen on monocytes and platelets was analyzed by FACS analysis and type I CD36-D was diagnosed by an absence of CD36 antigen in both cells. Statistical significance was assessed by Pearson's chi-square test using JMP 8 software (SAS Institute Japan, Tokyo, Japan).

Results

Case Presentations

Out of 40 patients with CD36-D, we experienced three representative cases of severe atherosclerotic cardiovascular diseases. The metabolic parameters of these patients are shown in **Table 1**, and compared with those of patients with CD36-D in our previous study[9]. As found in that study, these three cases were accompanied by hypertriglyceridemia and low HDL-C, and hypertension (Case 2 received anti-hypertensive drugs), while one case showed high fasting plasma glucose.

Case 1 is a 74-year-old man. At the age of 62, he suffered acute myocardial infarction. Coronary angiography demonstrated severe and diffuse stenoses in 3 major coronary arteries (**Fig. 1A** and **1B**) and he underwent percutaneous coronary revascularization. At the age of 66, angiographic restenosis was detected in the right coronary artery (RCA) and left anterior descending artery (LAD), which were later revascularized successfully. At the same time, we found total oc-

Advance Publication
Journal of Atherosclerosis and Thrombosis
Accepted for publication: September 6, 2011
Published online: November 10, 2011

Table 1. Metabolic Profiles of Three Cases of CD36-D Associated with Severe Atherosclerotic Cardiovascular Diseases

	Case 1	Case 2	Case 3	CD36-D ($n=40$)*	Healthy subjects ($n=84$)*
Age (year)	74	73	73	62±14	60±14
Sex (m/f)	male	male	female	(25, 15)	(63, 21)
BMI (kg/m^2)	21.6	24	21.4	23.5±3.6	23.5±2.0
TC (mg/dl)	193	166	220	201±39	205±32
TG (mg/dl)	192	152	156	178±89	126±62
HDL-C (mg/dl)	29	34	34	46±15	61±11
FPG (mg/dl)	100	87	210	110±22	95±18
sBP (mmHg)	152	128	154	135±18	115±15
dBP (mmHg)	94	86	53	80±10	77±18

*CD36-D ($n=40$) and healthy, age, sex, and BMI-matched controls ($n=84$) were quoted from our previous study (Reference 9).
Abbreviations: BMI, body mass index; TC, total cholesterol; TG, triglycerides; FPG, fasting plasma glucose; sBP, systolic blood pressure; dBP, diastolic blood pressure.

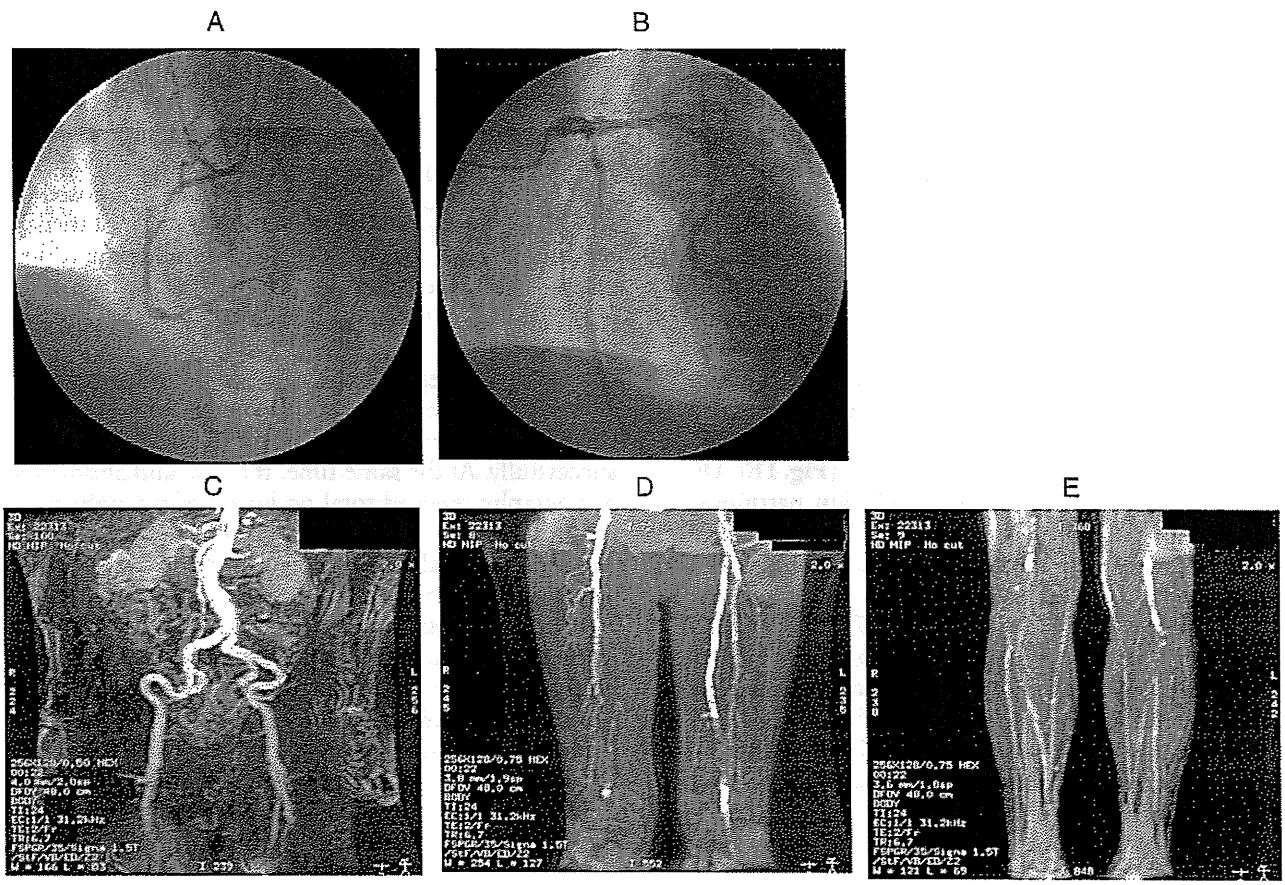

Fig. 1. Case 1, a 74-year-old male patient with CD36-D

At the age of 62, he suffered from acute myocardial infarction, and emergent cardiac catheterization revealed severe and diffuse stenosis in the triple coronary arteries (1-A, right coronary artery (RCA); 1-B, left coronary artery (LCA), respectively). Magnetic resonance angiography revealed total occlusion of bilateral femoral arteries (1-C and 1-D), total occlusion of left anterior tibial artery and severe stenosis of right anterior tibial artery (1-E).

Advance Publication
Journal of Atherosclerosis and Thrombosis
Accepted for publication: September 6, 2011
Published online: November 10, 2011

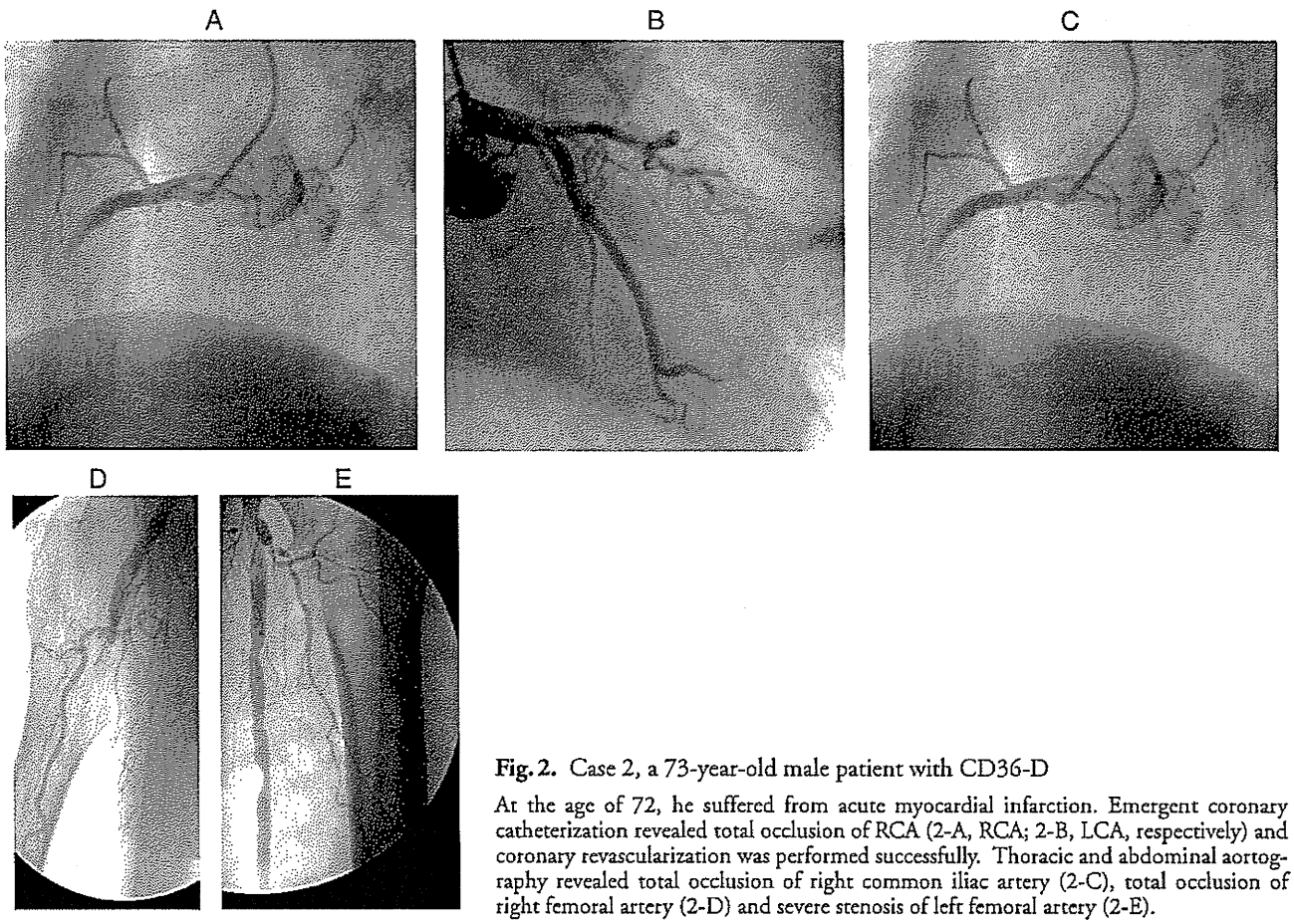

Fig. 2. Case 2, a 73-year-old male patient with CD36-D

At the age of 72, he suffered from acute myocardial infarction. Emergent coronary catheterization revealed total occlusion of RCA (2-A, RCA; 2-B, LCA, respectively) and coronary revascularization was performed successfully. Thoracic and abdominal aortography revealed total occlusion of right common iliac artery (2-C), total occlusion of right femoral artery (2-D) and severe stenosis of left femoral artery (2-E).

clusion of bilateral femoral arteries (**Fig. 1C** and **1D**), complete obstruction of the left anterior tibial artery and severe stenosis of the right anterior tibial artery by magnetic resonance angiography (MRA) (**Fig. 1E**). Up to the age of 73, the serum level of brain natriuretic peptide (BNP) gradually increased and left ventricular ejection fraction assessed by echocardiography gradually decreased, although repeated revascularization was undergone successfully. At the age of 74, ^{123}I-BMIPP scintigraphy revealed no myocardial uptake of BMIPP, an analogue of LCFA, and he was diagnosed with type I CD36-D by FACS analysis. Regarding his risk factors for cardiovascular diseases, he had a history of smoking and impaired glucose tolerance was observed by an oral glucose tolerance test (data not shown) in addition to the metabolic disorders shown in **Table 1**.

Case 2 is a 73 year-old man. He had a history of excessive alcohol consumption, but he had never smoked. For over 10 years he regularly attended Osaka University Hospital and received medical treatments for hypertension and intermittent claudication. At the age of 72, he suffered acute myocardial infarction. On emergent coronary angiography, total occlusion of RCA was identified (**Fig. 2A** and **2B**), and thereafter coronary revascularization was performed successfully. At the same time, thoracic and abdominal aortography revealed total occlusion of the right common iliac artery (**Fig. 2C**), complete obstruction of the right femoral artery (**Fig. 2D**) and severe stenosis of the left femoral artery (**Fig. 2E**). Thus, we decided to start anticoagulant therapy. Left ventricular ejection fraction in echocardiography did not improve although coronary revascularization was successful; therefore, we tested whether LCFA metabolism was impaired by scintigraphy using ^{123}I-BMIPP, an analogue of LCFA, and found marked reduction of myocardial uptake of ^{123}I-BMIPP. He was finally diagnosed with type I CD36-D by FACS analysis. This was accompanied by moderate hypertension and dyslipidemia, including hypertriglyceridemia and low HDL-C, as shown in **Table 1**.

Case 3 is a 73 year-old woman. She had no history of smoking or regular alcohol intake. At the age of 64, she began to feel chest discomfort and muscle

Advance Publication
Journal of Atherosclerosis and Thrombosis
Accepted for publication: September 6, 2011
Published online: November 10, 2011

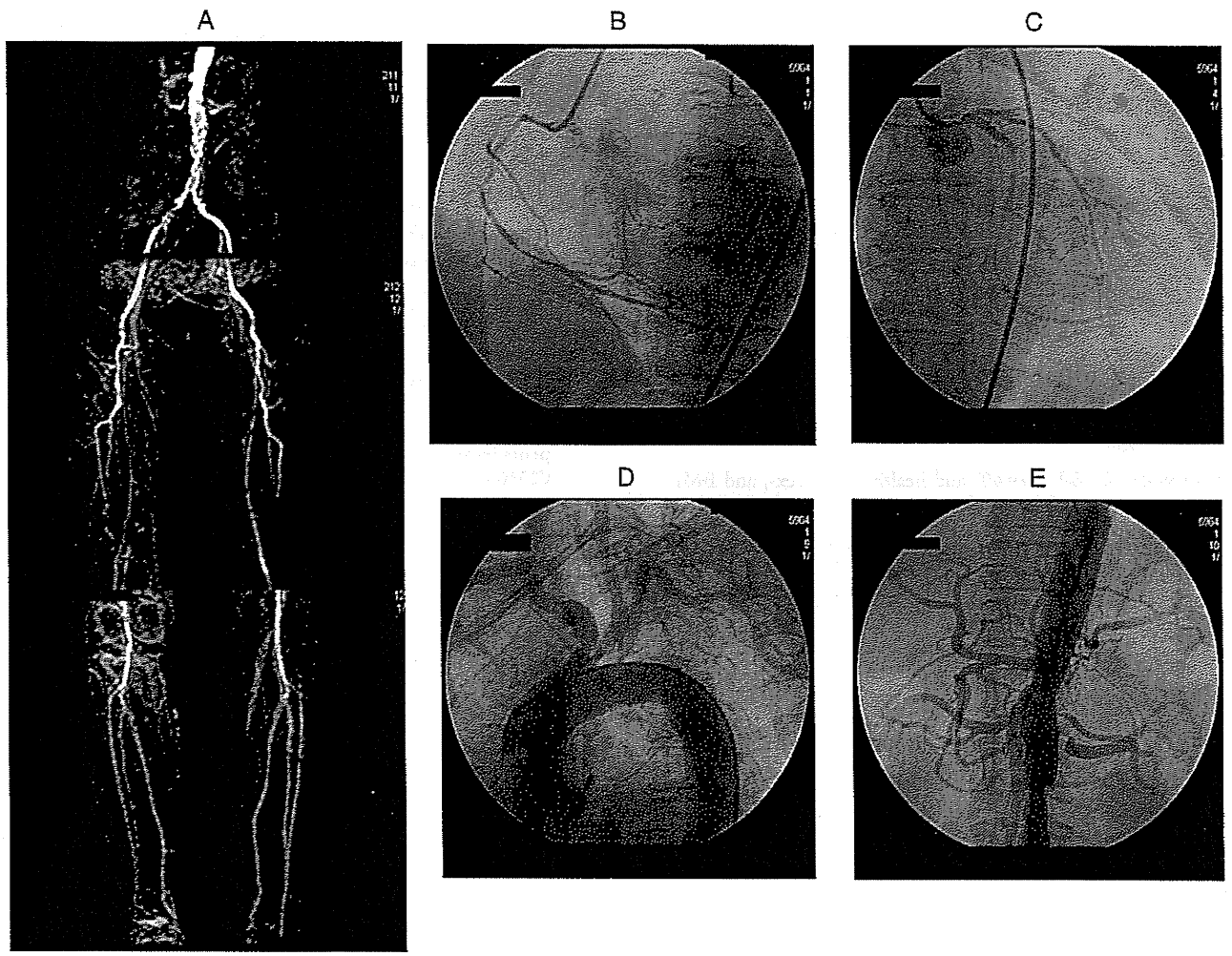

Fig. 3. Case 3, a 73-year-old female patient with CD36-D

At the age of 64, she felt chest discomfort and muscle fatigue of the bilateral legs after climbing stairs. Magnetic resonance angiography (MRA) of lower limbs revealed total occlusion of bilateral femoral arteries and severe stenosis of right common iliac artery and bilateral popliteal arteries (3-A). The following year she was hospitalized for refractory unstable angina, and diagnostic cardiac catheterization revealed severe stenosis of triple coronary arteries (3-B and 3-C). Thoracic and abdominal aortography revealed severe stenosis of trunks brachiocephalicus, right common carotid artery (3-D), abdominal aorta and left renal artery (3-E).

fatigue of the bilateral legs after climbing stairs. MRA of the lower limbs revealed total occlusion of the bilateral femoral arteries and severe stenosis of the right common iliac artery and bilateral popliteal arteries (**Fig. 3A**); therefore, anticoagulant drugs and vasodilators were administered. The following year she was hospitalized because of refractory unstable angina. Emergent diagnostic cardiac catheterization and thoracic and abdominal aortography were performed, which revealed severe stenoses of triple coronary arteries (**Fig. 3B** and **3C**), the brachiocephalic trunk, right common carotid artery (**Fig. 3D**), abdominal aorta and left renal artery (**Fig. 3E**). At the same time, the patient was diagnosed with type II diabetes, hypertension, hypertriglyceridemia and low HDL-C, and drug treatments were started for these diseases. After stent implantation in the left renal artery, coronary artery bypass graft surgery was performed and a saphenous vein graft was connected to the RCA and left circumflex coronary artery, and the left internal thoracic artery to LAD. At the age of 73, she began to complain of exertional dyspnea and the serum level of BNP gradually increased even though these grafts were patent and native coronary arteries remained intact, as assessed by coronary angiography. ^{123}I-BMIPP scintigraphy revealed no myocardial uptake of BMIPP and she

Advance Publication
Journal of Atherosclerosis and Thrombosis
Accepted for publication: September 6, 2011
Published online: November 10, 2011

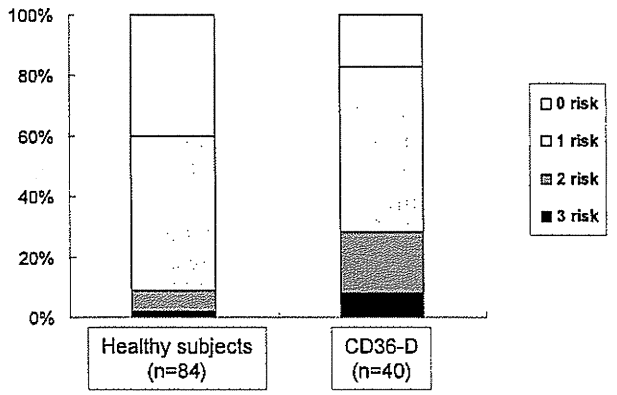

Fig. 4. Number of risk factors for CAD in patients with CD36-D

Patients with CD36-D (n=40) and healthy, age-, sex-, and BMI-matched controls (n=84) were from our previous study (Reference 9). Diabetes mellitus, hypertension and dyslipidemia were counted as risk factors for CAD. Patients with CD36-D had more risk factors for CAD than healthy subjects (patients with CD36-D vs healthy subjects: 1.20±0.80 vs 0.76±0.72 risk factors, P=0.005), and were associated with multiple risk factors for CAD.

was diagnosed with type I CD36-D by FACS analysis.

Number of Risk Factors for CAD in Patients with CD36-D and Healthy Control Subjects

We compared the number of risk factors for CAD in patients with CD36-D (n=40) and healthy, age, sex, and BMI-matched control subjects (n=84) from our former study[9]. These risk factors included diabetes mellitus, hypertension and dyslipidemia. As shown in **Fig. 4**, patients with CD36-D had more risk factors for CAD than healthy subjects (1.20±0.80 vs. 0.76±0.72 risks, p=0.005), and were often associated with multiple risk factors for CAD.

Frequency of CAD in Patients with CD36-D

The frequency of CAD was examined among 40 patients with CD36-D who were identified by an absence of cardiac uptake of ^{123}I-BMIPP. As shown in **Table 2**, the frequency of CAD in CD36-D patients was significantly high (50%, 20 of 40 CD36-D patients). Furthermore, in 20 CD36-D cases of CAD, coronary stenoses with high severity, acute or old myocardial infarction and unstable angina pectoris were observed in 65% (13 of 20 patients with CD36-D). These data suggest that CD36-D patients are accompanied by enhanced atherosclerotic cardiovascular diseases. By a screening study of FACS analysis, we found 8 patients with type I CD36 deficiency. Three patients (37.5%) out of 8 had coronary artery stenoses by coronary angiography.

Table 2. Frequency of Coronary Artery Disease in Patients with CD36 Deficiency

Patients with CD36-D (n=40)	
BMIPP	
CAD negative	50% (20/40)
CAD positive	50% (20/40)
acute MI	22.5% (9/40)
unstable angina	10% (4/40)
stable angina	17.5% (7/40)
Screening Study by FACS	
CAD negative	62.5% (5/8)
CAD positive	37.5% (3/8)

Abbreviations: BMIPP, ^{123}I-beta-methyl-p-iodophenyl-pentadecanoic acid; CAD, coronary artery disease; CD36-D, CD36 deficiency; MI, myocardial infarction.

Table 3. Frequency of CD36-D in Patients with Coronary Artery Disease

	Patients with CAD (n=319)	Healthy subjects (n=1239)
Frequency of CD36-D	0.94%* (3/319)	0.32% (4/1239)

*p<0.0001, assessed by Pearson's chi-square test

Prevalence of CD36-D in Patients with CAD and Healthy Subjects

In order to investigate whether CD36-D may increase the prevalence of CAD, we also compared the morbidity of CD36-D between healthy subjects (n=1,239) and patients with CAD diagnosed by coronary angiography (n=319). As shown in **Table 3**, the frequency of CD36-D in patients with CAD was approximately 3-fold higher than in healthy subjects [CAD patients vs healthy subjects, 0.94 % (3/319) vs 0.32 % (4/1239)]. The statistical significance was assessed by Pearson's chi-square test, and the frequency of CD36-D was significantly higher in patients with CAD (p<0.0001). These data suggest that patients with CD36-D are susceptible to CAD.

Discussion

In patients with CD36-D, compared with healthy CD36-positive controls, metabolic phenotypes such as high TG levels, low HDL-C levels, high fasting glucose and hypertension were observed more frequent-

Advance Publication
Journal of Atherosclerosis and Thrombosis
Accepted for publication: September 6, 2011
Published online: November 10, 2011

ly[7, 9]. Furthermore, we also found that patients with CD36-D are accompanied by insulin resistance[10], postprandial hyperlipidemia, and high levels of remnant lipoprotein cholesterol and FFA[8-9]. These coronary risk factors were clustered in each CD36-D patient, which may appear to be partly similar to the profiles of patients with MetS[8-9]. Another report showed that Pro90Ser CD36 mutation was associated with elevated FFA levels[19]. These profiles have been shown to be independent coronary risk factors by many clinical investigations[11-13]; however, the morbidity of atherosclerotic cardiovascular diseases in patients with CD36-D has not been clarified beside the reports of Ma *et al.*[20] and Yasunaga *et al.*[21]. Ma *et al*[20] showed that a common haplotype at the CD36 locus was associated with high FFA levels and increased cardiovascular risk in Caucasians. Yasunaga *et al.*[21] reported a 45-year-old male CD36-D patient with acute coronary syndrome without major cardiovascular risk factors. Emergency coronary angiography demonstrated 90% stenosis at segment 7 of LAD. We compared the number of risk factors for CAD in patients with CD36-D and healthy subjects (**Fig. 4**). Patients with CD36-D had more risk factors for CAD than healthy subjects and were associated with multiple risk factors for CAD. We also suggested that the clustering of coronary risk factors might increase the morbidity of cardiovascular disease in patients with CD36-D compared with healthy subjects.

In the current study, we investigated for the first time whether the morbidity of atherosclerotic cardiovascular diseases in CD36-D patients is higher. The clinical observations of three representative CD36-D patients were demonstrated in detail for those whose atherosclerotic lesions of not only coronary arteries but also the aorta and its branches could be assessed. As demonstrated in **Table 1**, dyslipidemia, hypertension and hyperglycemia were clustered in these three cases. Aortography and MRA revealed severe and multiple stenoses and occlusion of the aorta, its branches and arteries of lower limbs. We also found that atherosclerotic lesions were relatively long (up to 8-10 cm) and their collateral circulation was developed sufficiently. It was suggested that multiple and sequential stenoses along with long distance occlusion were not due to acute thrombotic occlusion but to chronic progression of atherosclerotic plaques. These three patients were rather older than the average CD36-D patients and were associated with multiple risk factors; therefore, we could not exclude the possibility that aging and the simple clustering of risk factors might have enhanced the atherogenicity in these three cases; however, a similar tendency of the clustering of CAD risk factors and the association of atherosclerotic cardiovascular diseases were also observed in younger patients with CD36-D.

We also investigated the morbidity and severity of atherosclerotic cardiovascular diseases in 40 patients with CD36-D who were identified by BMIPP scintigraphy and a screening study by FACS analysis. As shown in **Table 2**, we found extremely high morbidity of CAD (50%, 20 of 40 patients with CD36-D). Among 20 CD36-D patients with CAD, 13 (65%) were accompanied by unstable angina or acute myocardial infarction due to the stenosis and occlusion of coronary arteries; therefore, these data suggest that the morbidity and severity of CAD were significantly higher in patients with CD36-D than CD36-positive control subjects. Furthermore, many patients with both CD36-D and CAD suffered from other atherosclerotic cardiovascular diseases involving the stenosis and occlusion of arteries in the upper and lower limbs.

Since ^{123}I-BMIPP scintigraphy was performed in order to evaluate the myocardial damage of FFA metabolism in subjects with possible ischemic heart disease, the possibility could not be rejected that the 40 patients in the current study were extracted from a population with high morbidity of CAD. Watanabe *et al.*[22] also reported patients with type I and type II CD36-D, many of whom were accompanied by CAD or cardiomyopathy, although these patients were found by ^{123}I-BMIPP scintigraphy. Therefore, in the current study, we also examined the morbidity of CAD from a screening study. The morbidity of CAD was 50% in CD36-D patients identified by ^{123}I-BMIPP scintigraphy, while 37.5% (3 CAD of 8 CD36-D patients) in the population in the screening study. Although these data further imply that the morbidity of CAD in patients with CD36-D is definitely high, the possibility of patient selection bias cannot be excluded.

To explore further the contribution of CD36-D to the development of CAD in the general population, we compared by FACS analysis the frequency of CD36-D between patients with CAD diagnosed by coronary angiography (n=322) and non-CAD subjects (n=1,239). As shown in **Table 3**, the frequency of CD36-D was significantly three times higher in patients with CAD than in non-CAD subjects; therefore, the risk for the development of CAD is significantly higher in CD36-D patients, although the uptake of oxidized LDL *in vitro* is reduced in monocyte-derived macrophages.

Since foam cell formation by the uptake of oxidized LDL was shown to be reduced in monocyte-derived macrophages of CD36-D patients, it may be necessary to explore novel mechanisms for the en-

Advance Publication
Journal of Atherosclerosis and Thrombosis
Accepted for publication: September 6, 2011
Published online: November 10, 2011

hanced atherogenicity in a CD36-deficient condition. We will discuss these mechanisms in more detail as follows (**Fig. 5**):

1) Increased Lipoprotein Remnants and Postprandial Hyperlipidemia

In the postprandial state of CD36-D patients, we demonstrated that not only hypertriglyceridemia but also increased levels of apoB-48, chylomicron remnants, and small dense LDL were observed[9]. In our previous papers, we demonstrated that CD36-null mice showed higher TG concentrations in plasma and intestinal lymph than wild-type mice even in a high fat loading state, suggesting that CD36-null mice may have intestinal overproduction of chylomicrons and may be a good mouse model of postprandial hyperlipidemia[23-24]. Furthermore, patients with CD36-D were also associated with insulin resistance, as we reported[10]. These profiles associated with impaired lipid and glucose metabolism proved to be independent coronary risk factors in the general CD36-positive population[11-13]. Moreover, these profiles were linked; the increase in chylomicron remnants in the postprandial state was shown to be associated with insulin resistance[25]; the production of small dense LDL was shown to be associated with the impaired postprandial clearance of TG-rich lipoproteins including remnants[26-27]; the accumulation of TG-rich lipoproteins caused an increase in FFA levels; high levels of FFA may suppress lipoprotein lipase (LPL) activity and the clearance of TG-rich lipoproteins, resulting in increased remnants[28]. Therefore, these lipoprotein phenotypes clustered in patients with CD36-D might have a synergistic influence and enhance the cardiovascular risk. Furthermore, as nicely reviewed by Fujioka *et al.*[29], increased remnant lipoproteins (mainly chylomicron remnants) contribute to form atherosclerotic lesions through a variety of mechanisms. It was demonstrated that chylomicron remnants invade directly into the subendothelial spaces of arteries and are taken up by macrophages via several receptors, such as LDL receptor-related protein (LRP) or apoB-48 receptor, resulting in macrophage foam cell formation[30-33]. We reported that increased serum chylomicron remnants are directly associated with enhanced carotid atherosclerosis in subjects with apparently normal TG levels[34]. Chylomicron remnants induce the secretion of monocyte chemoattractant protein 1 (MCP-1), which stimulates the migration of monocytes through arterial endothelial layers[35] and the production of plasminogen activator inhibitor-I (PAI-I), which regulates thrombus formation on endothelial cells[33]. Thus, abundant chylomicron remnants in the blood of CD36-D patients might enhance the foam cell formation of CD36-deficient macrophages, leading to the development of atherosclerotic cardiovascular diseases.

2) Reduced Serum HDL-C Levels

In CD36-D patients, we demonstrated a reduction of serum HDL-C[9], although there is a report showing an increase of serum HDL-C[36]. More recently, Love-Gregory *et al.*[37] reported a homozygote of SNP32 who was CD36-D accompanied by hypertriglyceridemia and reduction of serum HDL-C, although heterozygotes showed an opposite profile. The reduced serum HDL-C in our CD36-D patients could be one of the causes of enhanced atherogenicity.

3) Increased Free Fatty Acids Levels Caused by Deficiency of LCFA Transporter

CD36 is distributed in the heart, skeletal muscles and adipose tissues where it functions as one of the transporters of LCFA[38]. CD36 may be a major transporter of LCFA in the heart, since the uptake of ^{123}I-BMIPP, an analogue of LCFA, in cardiac scintigraphy is markedly deficient in CD36-D patients, which causes increased serum FFA and the 2-fold-enhanced influx of LCFA into the liver[39]. Increased FFA flux into the liver may cause overproduction of VLDL and hypertriglyceridemia as well as insulin resistance.

4) Insulin Resistance and Impaired Glucose Metabolism

CD36-D was shown to be accompanied by insulin resistance[10, 40-43]; however, this is controversial[36, 44]. CD36 knockout mice developed marked glucose intolerance, hyperinsulinemia and decreased muscle glucose uptake on a fructose-rich diet, but not on a high-starch, low-fat diet[42]. Goudriaan *et al.*[43] demonstrated that CD36-D increases insulin sensitivity in muscle, but induces insulin resistance in the liver. Insulin resistance may lead to the down-regulation of lipoprotein lipase and finally to hypertriglyceridemia.

5) Hypertension

The average systolic and diastolic blood pressure in our CD36-D patients was significantly high compared with CD36-positive subjects, similar to the reported case of MetS and vasospastic angina[45]. The mechanism for increased blood pressure is unknown; however, it may accelerate the development of atherosclerosis.

6) Increased PAI-I Levels

Low plasma fibrinolytic activity in association with increased PAI-I levels has been demonstrated to